Doctoral Dissertation

# Exploring and Improving lung-targeting function of GALA peptide-modified lipid nanoparticle

## （GALA 修飾脂質ナノ粒子の肺標的化機能の評価および改良）

Laboratory of Molecular Design for Pharmaceutics

Major of Life Sciences　　Biomedical Course

Graduate School of Life Sciences,

Hokkaido University

Sarochin Santiwarangkool

September 2017

# Contents

# Figure contents

# Table contents

# Abbreviations

| | |
|---|---|
| ATI | Type I alveolar epithelium |
| ATIs | Type I alveolar epithelial cells |
| ATII | Type II alveolar epithelium |
| AuNPs | Gold nanoparticles |
| CTB | Cholera Toxin B |
| DiD | 1,1'-Dioctadecyl-3,3,3',3'-tetramethylindodicarbocyanine, 4-chlorobenzenesulfonate salt |
| DiI | 1,1'-Dioctadecyl-3,3,3',3'-tetramethyl indocarbocyanine perchlorate |
| DMG-$PEG_{2000}$ | 1,2-Dimyristoyl-sn-glycerol, methoxy polyethylene Glycol 2000 ether |
| DOTMA | 1,2-Di-O-octadecenyl-3-trimethylammonium propane (chloride salt) |
| DSG-$PEG_{2000}$ | 1,2-Distearoyl-sn-glycerol, methoxy polyethylene Glycol 2000 ether |
| DSG-$PEG_{2000}$-MAL | 1,2-Distearoyl-sn-glycero-N-[maleimide(polyethyleneglycol)-2000] |
| EC | Lung endothelium |
| ECs | Lung endothelial cells |
| $ED_{50}$ | 50% Effective dose |
| EPC | Egg phosphatidylcholine |
| GALA | GALA peptide (WEAALAEALAEALAEHLAEALAEALEALAA) |
| GALA/Chol | Cholesterol conjugate of GALA |
| GALA/PEG | PEGylated GALA (PEG conjugate of GALA) |
| HMVEC-L | Human lung microvascular endothelial cells |
| LPs | Liposomes |
| MEND | Multifunctional envelope-type nano device |
| miRNA | MicroRNA |
| PCR | Polymerase chain reaction |
| pDNA | Plasmid DNA |
| Pdpn | Podoplanin |
| PEG | Polyethylene glycol |
| RES | Reticuloendothelial systems |
| siRNA | Small-intefering RNA |
| STR-$PEG_{2000}$ | Stearyl-polyethylene glycol 2000 |
| *t*-BuOH | *tert*-Butyl ethanol |

# Introduction

# Introduction

According to the report by WHO, respiratory diseases were ranked in top 10 causes of death worldwide in 2000 and 2015 **(Figure 1)**.[1] Among respiratory disorders in the ranks, lower respiratory infections and chronic obstructive pulmonary diseases (COPD) were the leading cause in both years. In Japan, patients who had respiratory disorders were mostly diagnosed with pneumonia, COPD, and asthma.[2] According to the survey by Ministry of Health, Labour and Welfare from Japan, inpatients were the highest for pneumonia (34.4 thousand patients in 2014), whereas the majority of outpatients were diagnosed with asthma (127.6 thousand patients in 2014). Also, medical cost for respiratory diseases was occupied by 7.4% (2,177 billion yen) of total medical cost in the fiscal year 2014 **(Figure 2)**.[3] The medical cost for elderly patients (age over than 65 years old) reached 45.7% (995 billion yen) of the total cost for respiratory diseases. In contrast to high medical expenses, the number of patients who have been diagnosed with chronic respiratory illnesses (Asthma and COPD) and pulmonary malignant neoplasia was hardly shown the decreasing trend from 1996 to 2014 **(Figure 3)**. Given by these data, treatment for respiratory diseases becomes more challenging to enhance cost efficiency and improve the quality of life.

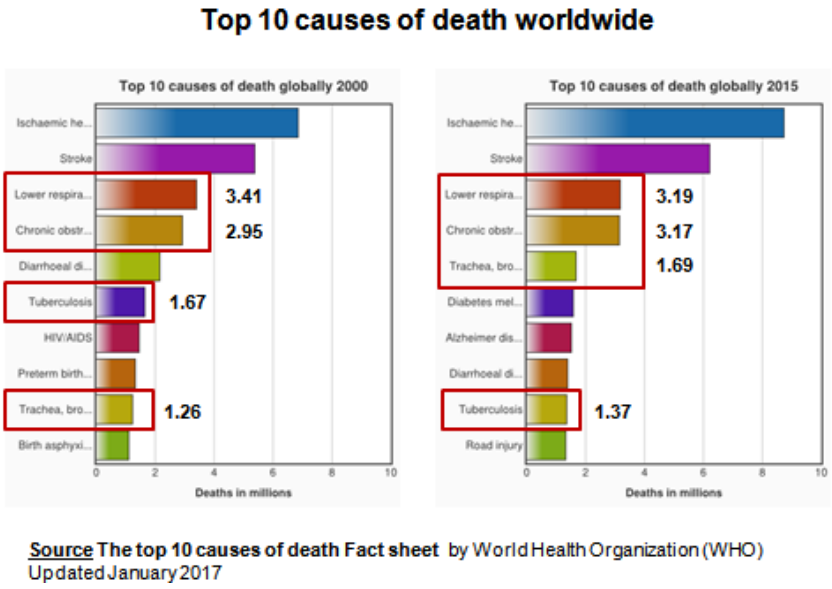


**Figure 1** Bar charts present top 10 causes of death worldwide in 2000 and 2015. (Adapted from [1])

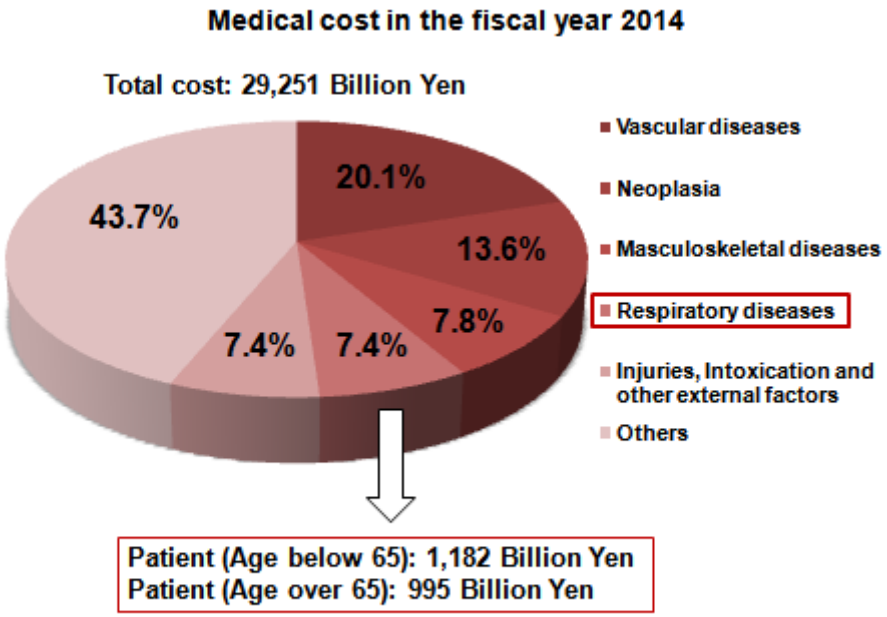


Source: 平成26年度 国民医療費の概況 (厚生労働省)

**Figure 2** A pie chart indicates medical cost in the fiscal year 2014. (Adapted from [3])

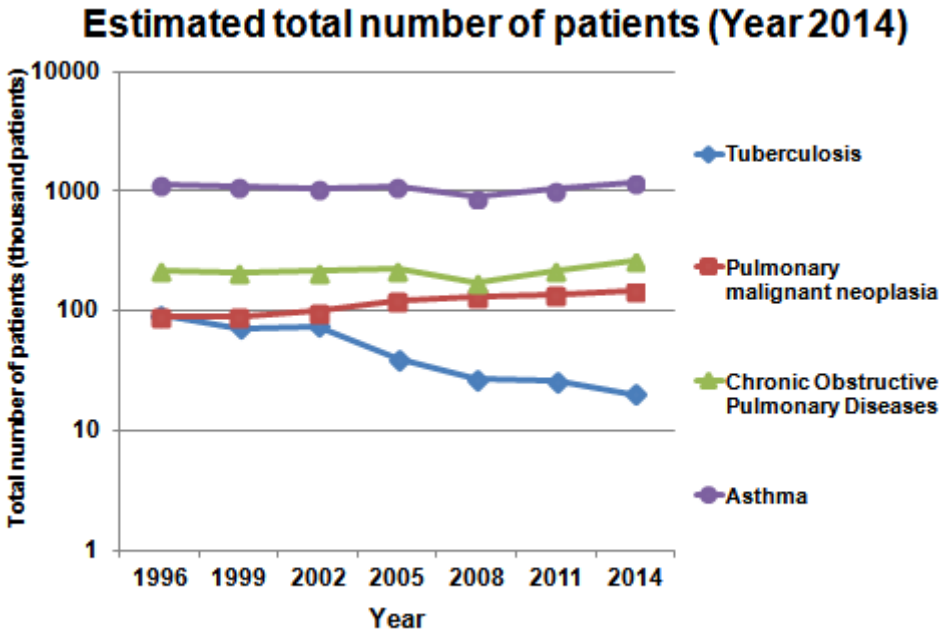


Source: 平成26年(2014)患者調査の概況 (厚生労働省)

**Figure 3** A line chart demonstrates estimated total number of patients with respiratory diseases in 2014. (Adapted from [2])

A lung plays a major role in the respiratory system by exchanging gas between the air and the blood circulation. The gas is conducted from the air to the lung via bronchial trees which include bronchi and bronchioles. Gas exchange subsequently occurs inside the subunit called, "alveolus" **(Figure 4)**. There is a gas-blood barrier inside this unit, by which contains thin layers of lung endothelium, a basement membrane, and an alveolar epithelium **(Figure 5)**. Because the barrier is merely thin as 0.1-0.5 μm, gas and nutrients could penetrate freely. The alveoli epithelia are classified into two types; type I alveolar cells which contain flat and large cytosol extensions, and type II alveolar cells which are cuboidal and include a large number of lamellar inclusion bodies. Type I alveolar cells take an essential function in gas exchange, occupying approximately 95% of the total alveolar epithelial surface area. In contrast, type II alveolar cells synthesize and secrete surfactant to maintain alveoli shape during breathing, covering only 5% of the surface area, but they represent 60% of the alveoli epithelium. The alveoli also contain other cell types that include alveolar macrophages, lymphocytes, plasma cells, neuroendocrine cells and plasma cells.[4-6]

The pulmonary vasculature contains approximately 30% of the endothelial surface in the body, in which becomes the major capillary network in the systemic circulation. The pulmonary vessels also play a pivotal role in supplying nutrients and oxygen throughout the body, because they receive more than 50% of the entire cardiac output. Therefore, relatively large blood supply is likely to provide benefits for pharmacological therapeutics due to the thorough distribution of drug compounds inside a lung.[8] Nevertheless, a little amount of the injected dose could be accumulated in the lung due to a lack of endothelial affinity. Several pharmacokinetic factors limit endothelial interactions of the drug, such as plasma protein binding, enzymatic degradation, clearance by reticuloendothelial systems.[9-11] Furthermore, even strong endothelial barriers which include adherence junctions, tight junctions, and a basement membrane impede endothelial permeation of macromolecules.[12] Nanocarriers are required to target lung endothelium directly so that drugs could be greatly accumulated in the lung.

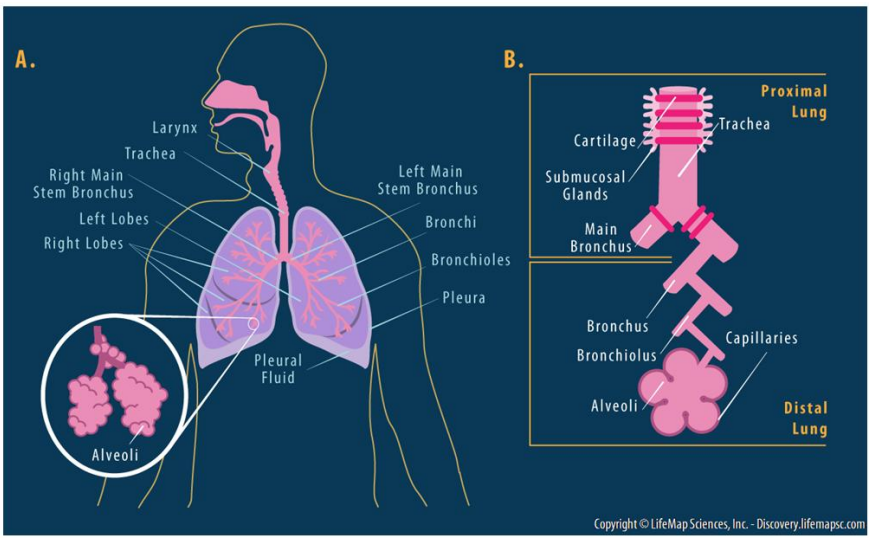


**Figure 4** Anatomical structure of lung (Taken from [7].)

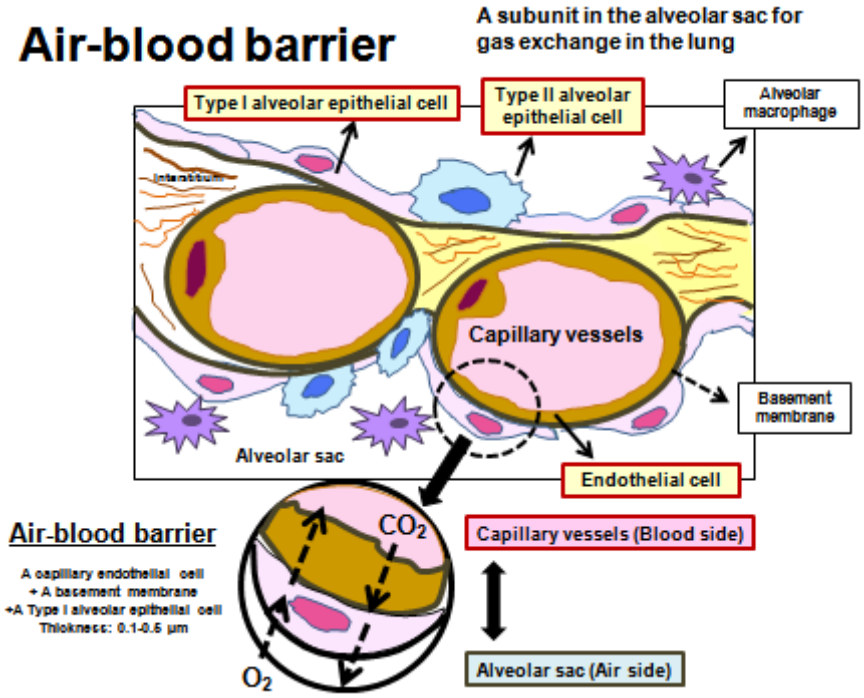


**Figure 5** A cross-sectional image of a blood-gas barrier inside the alveolus (Adapted from [6])

GALA peptide (WEAALAEALAEALAEHLAEALAEALEALAA) has been extensively used to improve intracellular delivery of nanocarriers, by promoting endosomal escape. Thus, compounds or macromolecules could be released efficiently from an endosome/lysosome.[13-18] Under physiological neutral pH, GALA maintains a random coiled structure. When pH turns acidic in the endosomal/lysosomal systems, its structure

changes from a random coil to an amphipathic α-helix that enables pore formation on the lipid bilayer **(Figure 6)**.[13,16] Consequently, the encapsulated compounds could be released prior to lysosomal degradation.

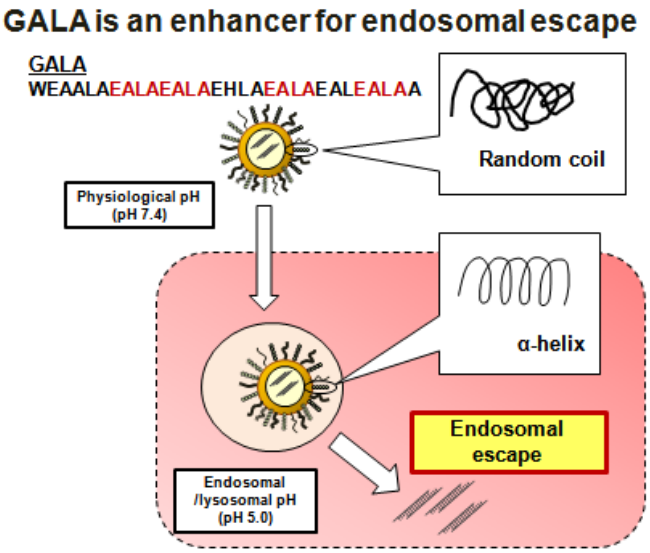


**Figure 6** An illustration represents endosomal escape activity of GALA

Recently, it has unexpectedly found that it functions as a targeting ligand to the lung endothelium.[19,20] GALA-modified liposomes (GALA-LPs) recognize patterns of sugar chains on the endothelial cell surfaces as likely as an influenza virus **(Figure 7)**. GALA-LPs could be retained the accumulation in the lung from 5 minutes up to 6 hours. When the liposomal nanocarrier: a multifunctional envelope-type nano device (MEND) which was encapsulated with siRNA was modified with GALA (GALA/MEND), silencing activity against the endothelial marker, CD31 was achieved in the lung endothelium.[19] Furthermore, GALA/MEND greatly inhibited lung metastasis in a melanoma-bearing mouse model. As a consequence, GALA becomes the potential candidate to develop lung-targeting nanocarriers.

In my Ph.D. dissertation, GALA was applied to design the nanocarriers with more efficient delivery to the lung. This work was separated into two major sections. For the first section, the topology of the GALA was examined for improving targeting activity to lung endothelium. This section further includes 2 parts; (1) the development of lung-targeting siRNA nanocarriers by the combination between GALA and a pH-sensitive lipid, YSK, and (2) the enhancement of lung-targeting activity by PEGylation. In another section, cellular

trafficking of GALA was investigated in detail. This section includes the elucidation of endocytosis mechanism and the evaluation of transendothelial activity in one part.

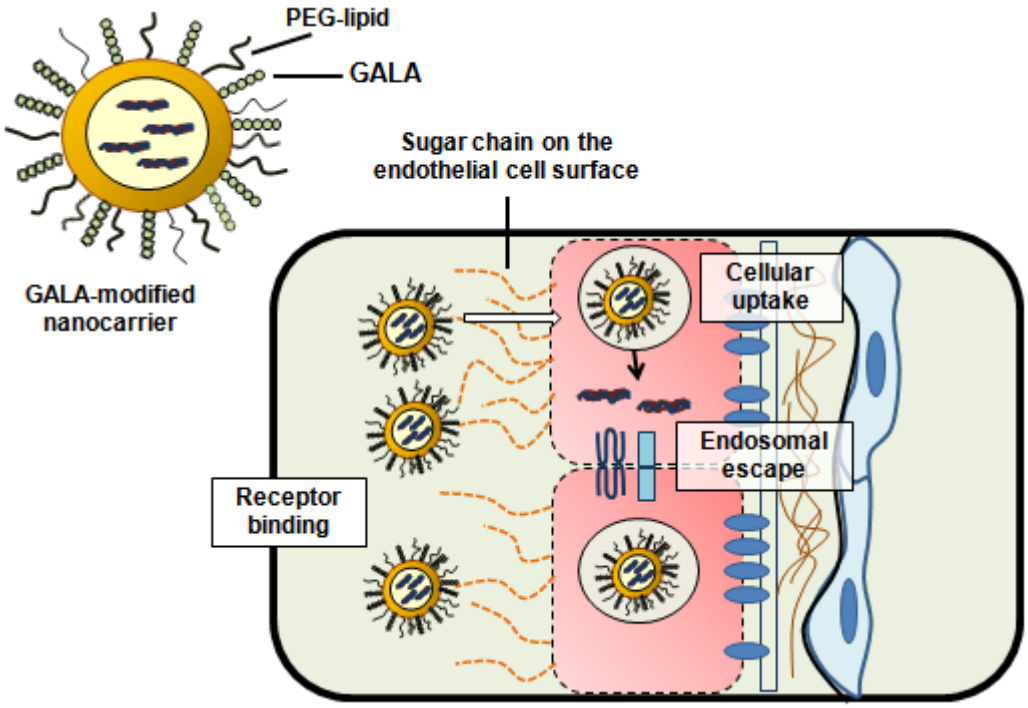


**Figure 7** An illustration represents the concept of a GALA-modified nanocarrier

# Chapter 1

# Lung-targeting siRNA nanocarriers by GALA and pH-sensitive lipid, YSK

# Chapter 1 Lung-targeting siRNA nanocarriers by GALA and pH-sensitive lipid, YSK

## 1.1 Introduction

Our laboratory has developed the liposome-based nanocarriers, called MEND by combining various functional ligands and lipids into the composition.[18] MENDs were reported for transporting nucleic acids such as pDNA[21,22], miRNA[23], and siRNA[24,25] effectively to many organs and promoting intracellular gene activity. GALA has been utilized for dual functions as an inducer of endosomal fusion[13,14,16] and a targeting ligand to lung endothelium[19,20]. GALA-modified MEND (GALA/MEND) was prepared by using a positively-charged lipid DOTMA as a main component. GALA/MEND which encapsulated siRNAs targeting an endothelial marker, CD31 showed the remarkable silencing function in lung endothelium.[19,20] More interestingly, it could strongly suppress lung metastasis of B16F10 melanoma cells after continuous administration.[20] GALA/MEND thus becomes the attracting choice for broad applications in respiratory diseases, such as lung cancer, pulmonary hypertension, acute lung injury.

DOTMA was reported for efficient gene transfection because it could promote the cellular uptake via electrostatic interactions between anionic charges from the cell membranes and cationic charges from the lipid molecules.[26,27] However, the cationic lipids have raised many questions regarding long-term safety for use. Elevation in inflammatory cytokines and infiltration of inflammatory immune cells was highlighted after using cationic lipoplexes.[28-30] Therefore, safety concerns would impede clinical applications in the long-term.

In our laboratory, a pH-sensitive lipid called YSK was synthesized to develop MENDs which obtain higher fusion activity. YSK possesses a neutral charge under a physiological pH (pH7.4) but becomes positively charged by acidification under an endosomal/lysosomal pH (pH5.0). The prototype lipid, YSK05, contains two unsaturated carbon chains and a pH-sensitive *N*-methyl piperidine group in which both are conjugated via acetal bond. At the endosomal pH, a cone-shaped structure of YSK05 is converted into an inverted hexagonal ($H_{II}$) phase so that membrane fusion could occur between the particle and

the endosome **(6).** As a consequence, The encapsulated compounds would be released prior to endosomal/lysosomal degradation.

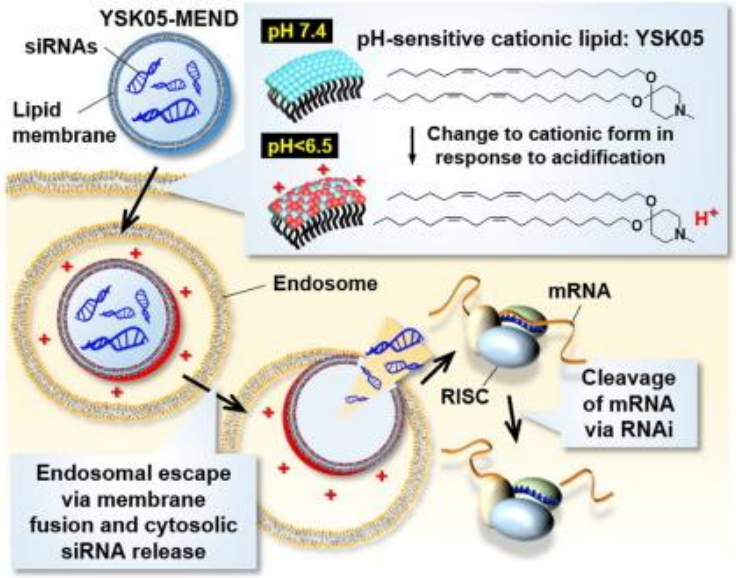


**Figure 1-1** Structure and functional mechanisms of YSK05 (Taken from [18])

YSK05 was shown for higher endosomal fusion ability than conventional cationic lipids.[25] Besides, a neutral charge is assumed to avoid inflammatory toxicities which were reported for cationic lipids. Thus, it is expected as the promising option for designing gene nanocarriers. YSK05 has been investigated for various pre-clinical applications. YSK05-MEND successfully transported miRNA into the hepatocytes and reduced blood cholesterol.[31] By modification with a tumor endothelium-targeting ligand, cRGD, YSK05-MEND robustly inhibited tumor growth and improved the distribution of lipid nanoparticles inside the tumor.[32,33] In addition, YSK05-liposomes which encapsulated cGMP efficiently induced production of type I interferon and activation of natural killer cells so that antitumor activity was exhibited in a lung metastasis model.[34]

In the 1$^{st}$ part, YSK05 was combined with GALA to develop a potent lung-targeting siRNA carrier GALA/YSK05-MEND. The aim of this part was focused on improving the intracellular trafficking of encapsulated siRNA in lung endothelium.

## 1.2 Materials and methods

### 1.2.1 Materials

GALA peptide (WEAALAEALAEALAEHLAEALAEALEALAA) was purchased from PolyPeptide Laboratories (San Diego, CA, USA). YSK05 was synthesized and purified as previously reported.[25] Cholesterol was ordered from AVANTI Polar Lipids (Alabaster, AL, USA). 1,2-Dimyristoyl-sn-glycerol, methoxy polyethylene Glycol 2000 ether (DMG-$PEG_{2000}$), 1,2-Distearoyl-sn-glycerol, methoxy polyethylene Glycol 2000 ether (DSG-$PEG_{2000}$), egg phosphatidylcholine (EPC) was purchased from NOF Corporation (Tokyo, Japan). Stearyl-polyethylene glycol 2000 (STR-$PEG_{2000}$) was purchased from Wako Pure Chemicals (Osaka, Japan). 1,1'-Dioctadecyl-3,3,3',3'-tetramethylindodicarbocyanine, 4-chlorobenzene sulfonate salt (DiD), Trizol® Reagent and Quant-iT$^{TM}$ RiboGreen assay were purchased from Thermo Fisher Scientific, Inc. (Waltham, MA, USA). Thunderbird$^{TM}$ SYBR® qPCR Mix and ReverTra Ace® qPCR RT Master Mix with gDNA Remover was purchased from Toyobo Co., Ltd. (Osaka, Japan). Triton X-100 was purchased from Sigma-Aldrich (St. Louis, MO, USA. Glycogen (M.B.) was acquired from GMbiolab Co., Ltd. (Taichung, Taiwan).

### 1.2.2 Mouse

Male C57BL6/J mice (6-8 weeks of age, 20-25 grams) were purchased from Nihon Clea Co., Ltd. (Tokyo, Japan).

### 1.2.3 siRNA sequences

CD31-targeting siRNAs were ordered from Hokkaido Bioscience Systems (Hokkaido, Japan; Table 1-1).

**Table 1-1** The sequences of CD31-targeting siRNAs

| siRNA name | Sequences (5'→3') | Molecular weight (g/mole) | Length (mer) | Tm (ºC) |
|---|---|---|---|---|
| CD31 | Sense: GUGCAUAGUUCAAGUGACATT | 6693.28 | 21 | 52.6 |
| | Antisense: UGUCACUUGAACUAUGCACTT | 6590.03 | 21 | N/A |

### 1.2.4 Preparation of GALA/YSK05-MEND

YSK05-MEND included YSK05 and cholesterol at the 7:3 molar ratio. PEG-lipids (STR-$PEG_{2000}$, DMG-$mPEG_{2000}$ or DSG-$mPEG_{2000}$) were added at 6 mole% to stabilize YSK05-MEND. 1,1'-dioctadecyl-3,3,3',3'-tetramethylindodicarbocyanine,4-chlorobenzenesulfonate (DiD) was added at 2.5 mole% to label the lipid. The lipid solution was diluted to 3.75 mM with 90% (v/v) *t*-BuOH. Then, 3 nmole of CD31 siRNA was diluted to 200 µg/mL with deionized distilled water. The siRNA solution was then mixed dropwise with the lipid solution under vigorous mixing. The lipid/siRNA molar ratio was fixed at 500. After mixing for 10 seconds, the siRNA-lipid mixture solution was transferred into 2 mL of citric acid buffer (pH 4.0; 20 mM) via a 27G-needle. Next, the solution was diluted with 3.5 mL of PBS(-) and transferred to a 50-mL Amicon tube. Seven mL of PBS(-) was further added into the tube. Ultrafiltration removed residual *t*-BuOH in the solution by using with Him CP702 centrifuge (Hitachi, Japan) under the following condition; 1000g, 25ºC, 12-15 minutes. 10 mL of PBS(-) was re-added into the tube to repeat washing *t*-BuOH, and the solution was concentrated under the same condition. Finally, the concentrated was diluted with PBS(-) to obtain siRNA concentration of 0.1 µg/µL. For post-modification of GALA, GALA/Chol was added at 2 mole% into MEND solution under the vigorous mixing. The solution was incubated in the shaking incubation under the following condition, 1000g, 25ºC, 30 minutes. Size and zeta potential were measured with Nano-ZS Zeta Sizer (Malvern instrument, UK).

### 1.2.5 Measurement of siRNA encapsulation efficiency

siRNA encapsulation efficiency and recovery ratio were quantitatively measured with Quant-iT$^{TM}$ RiboGreen assay. The mixture1 solution included dextran sulfate (20 µg/mL) and Ribogreen (5:1000 by volume). Triton X-100 (0.1% w/v) was added to the mixture1 solution to prepare the mixture2 solution. The mixture solution was separately mixed with diluted MEND solution at 1:1 volume ratio. Fluorescent intensity from Ribogreen was measured by the fluorescent plate reader (EnSpire 2300 multilabel reader; Perkin Elmer, Waltham, MA, USA). Encapsulation efficiency and recovery ratio was calculated with the following formula;

siRNA encapsulation efficiency (%) =

$$\frac{\text{(siRNA concentration from the mixture2 - siRNA concentration from the mixture 1)}}{\text{siRNA concentration from the mixture2 solution}} \times 100$$

**1.2.6 Intravenous administration of MEND**

MEND was injected intravenously at the siRNA doses of 0.01-0.2 mg/kg via a tail vein. At 24 hours after administration, mice were sacrificed to collect organ tissues into the Eppendorf tubes and were frozen in liquid nitrogen. Organ tissues were sampled 30-40 mg or as a whole for RNA extraction, and were stored at - $80^0$C.

**1.2.7 RNA extraction**

Lung samples were thawed at room temperature. RNA extraction was conducted by using Trizol® reagent under the manufacture's protocol. After extraction, RNA samples were purified by ethanol precipitation. Final RNA concentration was measured with a UV spectrophotometer (Nanodrop; Thermo Fisher Scientific, Inc., Massachusetts, USA).

**1.2.8 Reverse transcription**

RNA solution equivalent to 250 or 500 ng RNA was diluted with RNase-free water up to 3 or 6 µL in a PCR tube. Reverse transcription was done by using ReverTra Ace® qPCR RT Master Mix with gDNA Remover and S1000 Thermal cycler (Bio-rad Laboratories, USA) and following the manufacture's protocol.

**1.2.9 Quantitative PCR using the comparative Ct method (ΔΔCt method)**

For each well, cDNA solution was diluted to 2.5 ng/µL with filtered (0.2 µm) deionized distilled water. 1 µL of diluted cDNA solution was mixed with 4 µL of primer mixture solution (625 nM) which consisted of the following components; Thunderbird™ SYBR® qPCR Mix 2.5 µL, primers (10 µM) 0.5 µL and DDW 1.5 µL. The mixture was added into LightCycler® 480 Multiwell Plate 384; Clear (Roche Diagnostics, Basel, Switzerland). PCR was conducted with LightCycler® 480 Instrument II, 384-well (Roche Diagnostics, Basel, Switzerland) under the following conditions;

| | | |
|---|---|---|
| Pre-incubation | 1 cycle: | 95ºC, 1 minute |
| Amplification | 40 cycles: | 95ºC, 15 seconds |

| | | |
|---|---|---|
| | | 55ºC, 30 seconds |
| | | 60ºC, 30 seconds |
| Melting curve | 1 cycle: | 95ºC, 5 seconds |
| | | 65ºC, 1 minute |
| | | 97ºC, cont |
| Cooling | | 40ºC, 15 seconds |

Gene expression was analyzed by the ΔΔCt method, comparing to GAPDH as a reference gene. The sequences of primers are shown in **Table 1-2**.

**Table 1-2** Sequences of CD31- and GADPH-targeting primers

| Primer name | Sequences (5'→3') | Molecular weight (g/mole) | Length (mer) | Tm (ºC) |
|---|---|---|---|---|
| CD31 F1 | TACAGTGGACACTACACCTG | 6086.0 | 20 | 55.9 |
| CD31 R1 | GACTGGAGGAGAACTCTAAC | 6175.1 | 20 | 54.3 |
| GAPDH F1 | AGCAAGGACACTGAGCAAG | 5879.9 | 20 | 60.8 |
| GAPDH R1 | TAGGCCCCTCCTGTTATTATG | 6363.2 | 20 | 61.6 |

**1.2.10 Evaluation of tissue accumulation**

The DiD-labeled MENDs were intravenously administered at the siRNA amount of 4 μg. At the certain interval, mice were sacrificed by $CO_2$ asphyxiation. Lungs and livers were collected and kept on ice until use. Lung and liver tissues were minced with scissors and transferred approximately 25 mg into the microtube (SARSTEDT, Germany). 10% (w/v) SDS solution in PBS(-) (1:9 by volume) was added to 600 μL per tube. The tissues were homogenized with Micro SmashTM MS-100R homogenizer (Tomy Medico, Japan) at $4^0$C, 6000 rpm for 60 seconds. All homogenates were centrifuged at $4^0$C, 15000 rpm for 5 minutes. Then, 200 μL of supernatant was taken to measure DiD fluorescent intensity with EnSpire 2300 multilabel reader (Perkin Elmer, USA). Tissue accumulation of the MENDs was calculated as % ID/g tissue, based on the standard calibration curve of DiD fluorescent intensity from the liposomes.

**1.2.12 Evaluation of blood retention**

Blood was drawn from inferior vena cava by a 1-mL syringe with the heparin-coated 26G-needle and kept at room temperature until use. 25 μL of blood sample was mixed with

225 μL of 10% (w/v) SDS solution in PBS(-) (1:8 by volume). 200 μL of the samples was taken to measure DiD fluorescent intensity with EnSpire 2300 multilabel reader (Perkin Elmer, USA). Blood retention of the MENDs was calculated as % ID/mL blood, based on the standard calibration curve of DiD fluorescent intensity from the liposomes.

## 1.3 Results

### 1.3.1 Optimizing PEG-lipid for GALA/YSK-MENDs

To stabilize the MENDs, a series of PEG was added to the lipid composition prior to preparation. PEG was widely reported to prolong blood retention by preventing protein adsorption (termed "opsonization") and RES uptake.[35-39] However, PEGylation could impede cellular uptake and endosomal escape, in which is termed "PEG dilemma."[14,38,40,41] Therefore, PEG-lipids were evaluated for effective silencing effect as well as reduced PEG dilemma effect. Three types of PEG-lipid with different acyl chains and carbon atoms were tested; STR-mPEG$_{2000}$ ($C_{18}$) which contains a single acyl tail, DMG-($C_{16}$) and DSG-mPEG$_{2000}$ ($C_{18}$) which both contain a double acyl tail **(Figure 1-2)**.

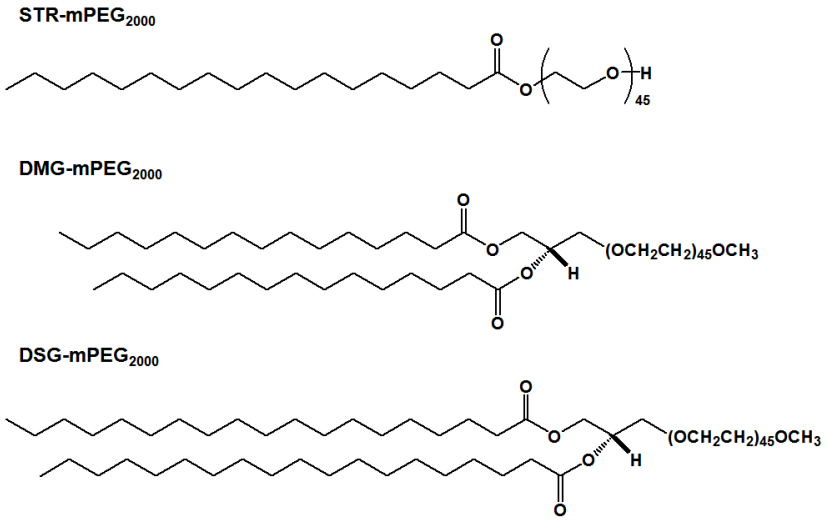


**Figure 1-2** Molecular structures of PEG-lipids used in the study; (A) STR-mPEG$_{2000}$, (B) DMG-mPEG$_{2000}$ and (C) DSG-mPEG$_{2000}$

Modification with STR-mPEG$_{2000}$ provided GALA/YSK05-MEND with a particle size more than 100 nm, while including DMG- and DSG-mPEG$_{2000}$ controlled the size to less than 100 nm **(Table 1-3)**. In the meanwhile, polydispersity index became relatively larger by DMG- or DSG-mPEG$_{2000}$, indicating that smaller particles with various size distribution were formed. Zeta potential showed the inverse correlation with size. GALA/YSK05-MEND had the lowest zeta potential after including STR-mPEG$_{2000}$, whereas it became less negative by inserting DMG- or DSG-mPEG$_{2000}$. It suggested that diacylglycerol conjugates of PEG

(DMG- or DSG-mPEG$_{2000}$) shield the negative charges of GALA more efficiently than the mono glycerol conjugate (STR-mPEG$_{2000}$). Compared to DMG-mPEG$_{2000}$, DSG-mPEG$_{2000}$ which contains more carbon atoms in an acyl backbone provided the carrier with less negative charge. Therefore, diacylglycerol-PEG derivatives with more carbon atoms tend to conceal the surface charge.

**Table 1-3** Physical characteristics of GALA/YSK-MEND with different types of PEG-lipids (n=1)

| GALA/ YSK05-MEND | Size (nm) | PDI | Zeta potential (mV) | siRNA encapsulation (%) |
|---|---|---|---|---|
| STR-mPEG$_{2000}$ | 131.8 | 0.200 | -15.2 | 79.6 |
| DMG-mPEG$_{2000}$ | 95.70 | 0.361 | -6.87 | 84.6 |
| DSG-mPEG$_{2000}$ | 85.76 | 0.345 | -1.82 | 87.6 |

Silencing effect of GALA/YSK05-MEND was evaluated for an endothelial marker, CD31 in lungs at the siRNA dose of 0.04 mg/kg. The maximal activity was obtained when STR-mPEG$_{2000}$ was incorporated into GALA/YSK05-MEND **(Figure 1-3).** mRNA expression of lung CD31 reduced by 42% for with GALA/YSK05-MEND modified with STR-mPEG$_{2000}$. However, the silencing activity was not observed in the case of inserting either DMG-PEG$_{2000}$ or DSG-PEG$_{2000}$. It was suggested that a single acyl chain of STR-mPEG$_{2000}$ facilitated intracellular activity by GALA/YSK05-MEND.

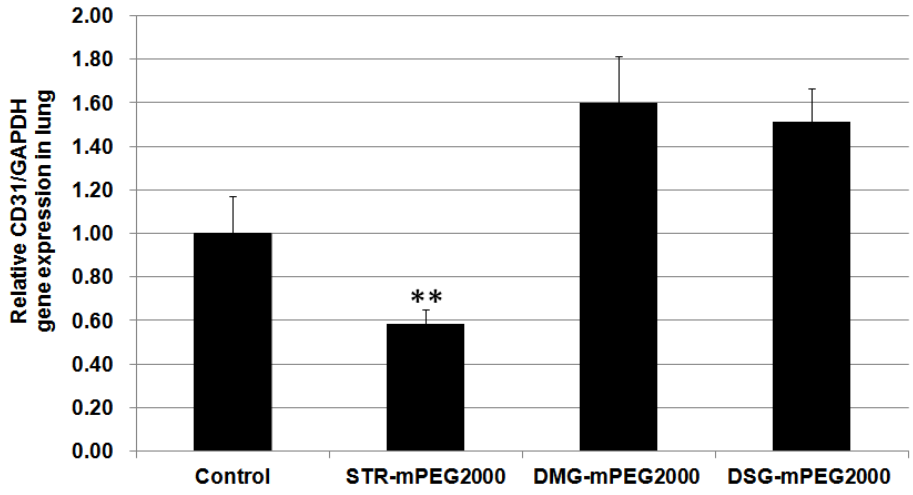

**Figure 1-3** Silencing activity against lung CD31 by GALA/YSK05-MENDs modified with different PEG-lipids. Data were represented as mean ± SD. (n = 3-4) **p<0.01 vs. control; One-way ANOVA followed by Bonferroni's test

### 1.3.2 Dose-dependent activity of GALA/YSK05-MEND

After optimizing GALA/YSK-MEND by including YSK05 and STR-mPEG$_{2000}$ into the lipid components, a dose-dependent pattern of silencing effect was evaluated *in vivo* in the dose range of 0.01-0.2 mg/kg. In the lung, GALA/YSK05-MEND showed the dose-response activity with the $ED_{50}$ value of 0.044 mg/kg **(Red line; Figure 1-4)**. The GALA/MEND containing DOTMA was previously reported for inducing the gene silencing with the $ED_{50}$ value of 0.17 mg/kg **(Black line; Figure 1-4)**[20]. Thus, introducing YSK05 improved silencing activity of GALA/MEND by 3.9 fold in the lung endothelium.

Anyway, silencing effect was also observed in liver endothelium with the $ED_{50}$ value of 0.045 mg/kg **(Figure 1-5)**. It indicated non-specific function of GALA/YSK05-MEND in other organs.

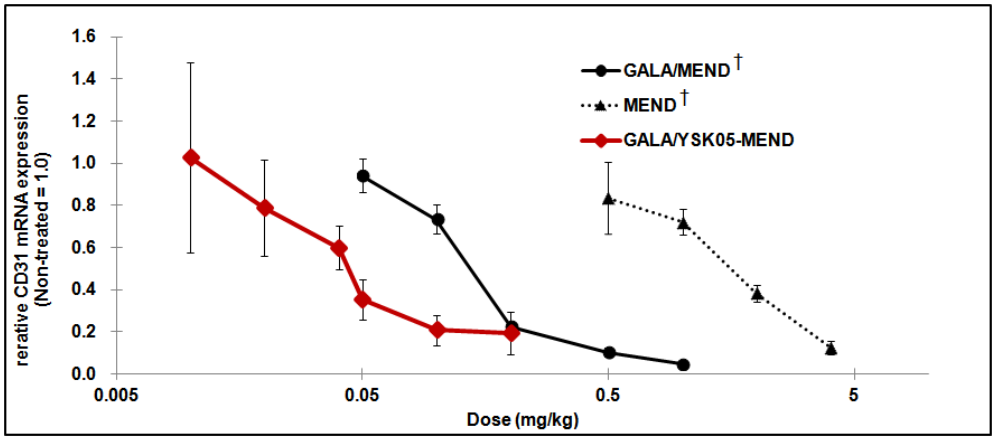


**Figure 1-4** Dose-response curve of silencing effect against lung CD31 by GALA/YSK05-MEND (red line). Data were represented as mean ± SD. (n = 7-8)

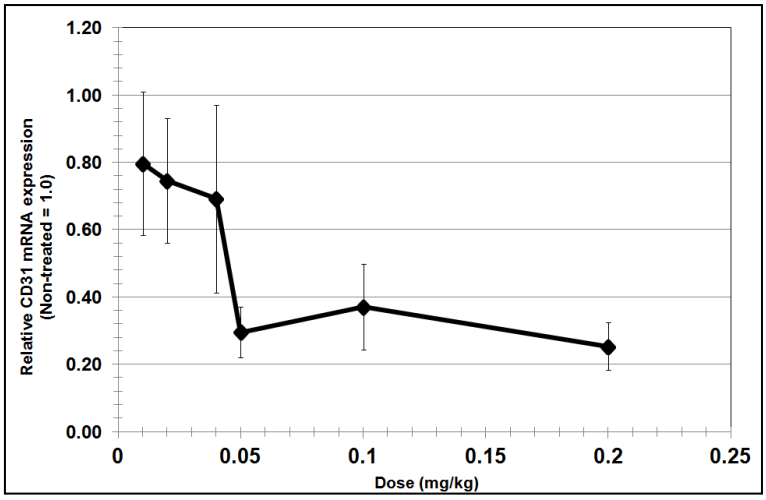


**Figure 1-5** Dose-response curve of silencing effect against liver CD31 by GALA/YSK05-MEND. Data were represented as mean ± SD. (n = 6-8)

### 1.3.3 Biodistribution of GALA/YSK05-MEND

Pharmacokinetic profiles were compared between GALA/YSK05-MEND and the unmodified YSK05-MEND at three points of intervals (1, 6 and 24 hours). DiD-labeled MENDs were intravenously administered at siRNA dose of 4 μg per mouse. Biodistribution in lungs, livers, and blood was evaluated by measuring DiD fluorescence intensity from the lipid with a UV spectrophotometer. As a result, lung accumulation of GALA/YSK05-MEND reached the maximum at 1-hour post-administration. GALA/YSK05-MEND showed the greater extent of lung accumulation than YSK05-MEND by up to 11.3 fold **(Figure 1-6A)**. Then, it gradually decreased over time from 37.0% ID/g tissue at 1 hour to 22.3% ID/g tissue at 24 hours. Blood retention of GALA/YSK05-MEND was also longer than YSK05-MEND by up to 4.1 fold **(Figure 1-6C)**. Blood concentration of GALA/YSK05-MEND reached the peak at the 1$^{st}$ hour at 24.0% ID/mL blood and rapidly decreased to lower than 10%ID/mL blood at 24 hours. In contrast, GALA/YSK05-MEND had a lower accumulation in the liver than YSK05-MEND by 2.7 fold **(Figure 1-6B)**. Liver accumulation of GALA/YSK05-MEND remained stable at 25-30% ID/g tissue up to 24 hours, whereas the accumulation amount of YSK05-MEND started to decline at 6-hour post-administration.

According to the data, the GALA modification could largely shift the accumulation of YSK05-MEND from the liver to the lung.

(A)

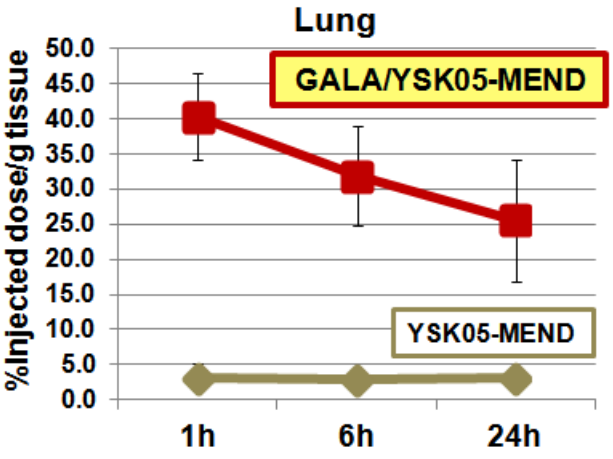


(B)

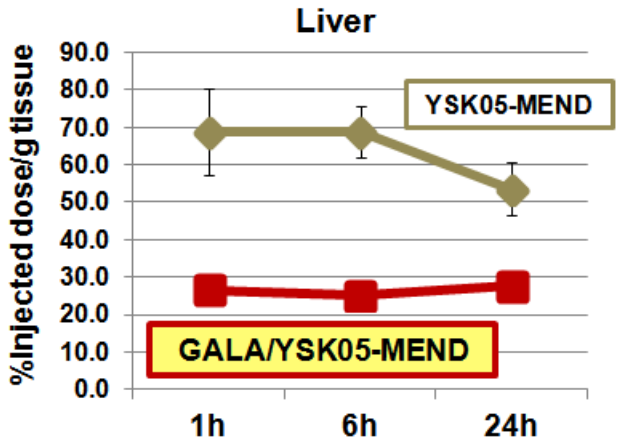


(C)

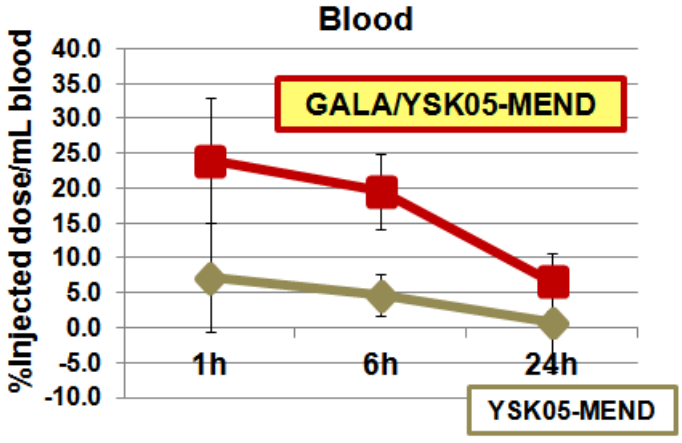


**Figure 1-6** *In vivo* biodistribution of GALA/YSK05-MEND and YSK05-MEND in lungs, livers and blood at 1, 6 and 24 hours. Data were represented as mean ± SD. (n = 6-7)

**1.4 Discussion**

GALA was combined with a pH-sensitive lipid, YSK to prepare the lung-targeting siRNA nanocarriers, GALA/YSK-MEND. The 1st generation lipid, YSK05 possessed efficient endosomal escape, resulting in surpassing conventional cationic lipid at greater silencing activity.[25] GALA exhibited dual functions as an inducer of endosomal escape and a targeting ligand to lung endothelium.[13,14,19] The combination of GALA and YSK05 was expected to improve the intracellular activity of siRNA by increasing endosomal escape inside lung endothelial cells.

GALA/YSK05-MEND was prepared with different kinds of PEG-lipid derivatives for optimization; STR-mPEG$_{2000}$, DMG-mPEG$_{2000}$ and DSG-mPEG$_{2000}$. The greatest gene silencing in the lung was found when GALA/YSK05-MEND was modified with monoacylglycerol PEG conjugate, STR-mPEG$_{2000}$ **(Figure 1-3)**. Such activity was not observed when the diacylglycerol conjugate, DMG- or DSG-mPEG$_{2000}$ was included into the MEND composition. These results concur well with the previous findings which have shown that, reducing the number of acyl chains from double to single improved the transfection activity of the carrier.[42] The most likely explanation is that mono stearyl chain enhances the dissociation of PEG in the endosome so that PEG dilemma could be avoided.[42] Besides, STR-mPEG$_{2000}$ led to superior lung distribution of GALA/MEND to the diacylglycerol-PEG (DSPE-mPEG$_{2000}$).[43] Therefore, STR-mPEG$_{2000}$ was chosen as the stabilizer of GALA/YSK05-MEND.

The optimized GALA/YSK05-MEND was examined for dose-dependent silencing activity. After exploring the dose-response plot, ED$_{50}$ of GALA/YSK05-MEND was estimated at 0.044 mg/kg **(Figure 1-4)**. Compared to the GALA/MEND which was previously reported by Kusumoto et al.[20], the silencing activity was enhanced by 3.9 fold. For the conventional GALA/MEND, a permanently-ionized lipid, DOTMA, was included in the lipid composition. The superiority of YSK05 to DOTMA in silencing activity could be explained by differences in molecular structures. Both DOTMA and YSK05 have two aliphatic chains which contain symmetric 18 carbon atoms on each.[44,45] However, they differ from linker structures and amino-based hydrophilic tails. DOTMA consists two ether bonds which are

linked to the quaternary ammonium head group[45], whereas YSK05 includes two acetal bonds which are in proximity with a heterocyclic ring, piperidine. [44] The acetal bond is an acid-sensitive linkage which could be degraded in the endosomes/lysosomes via hydrolysis.[46,47] On the contrary, the ether bond is stable from the acidic hydrolysis.[48] Acetal bonds from YSK05 are thus likely to be cleaved more easily than ether bonds from DOTMA under the endosomal/lysosomal pH. In addition, the degree of saturation in hydrophobic tails was reported for influence on membrane fusion activity. Unsaturated lipids which contain a higher number of double bonds undergo a transition to inverted hexagonal (HII) phase more efficiently than either saturated or less unsaturated lipids, due to lower phase transition temperature.[49] As a consequence, bilayer rigidity would be reduced, and membrane destabilization is more likely to occur.[50,51] Since YSK05 contains a larger number of double bonds than DOTMA[25,45], YSK05 is supposed to adopt more effective and rapid membrane fusion than DOTMA does. Therefore, the molecular structure of YSK05 is expected to potentiate the intracellular activity of GALA/YSK05-MEND in lung endothelium.

However, silencing function of GALA/YSK05-MEND would not be specific for any organs, as the silencing activity was observed in liver endothelium **(Figure 1-5)**. Previous reports revealed that neutral lipid particles were taken up into a liver in an Apolipoprotein E (ApoE)-dependent manner.[52,53] In general, ApoE functions lipid transport in cells via the low-density lipoprotein (LDL) receptor family.[54] Furthermore, sinusoidal endothelial cells (SECs) also express a low-density lipoprotein receptor-related protein-1 (LRP-1).[55] YSK05 is neutrally-charged at physiological pH (pH 7.4), GALA/YSK05-MEND might be incorporated to ApoE and carried to liver capillaries via LRP-1 binding. This phenomenon would possibly promote silencing activity against liver CD31. Given these data, GALA/YSK05-MEND is likely to target other organs rather than a lung. Silencing effect will be further investigated to discover applications of GALA/YSK05-MEND in other organs.

Organ distribution of GALA/YSK05-MEND and YSK05-MEND was evaluated in lung, liver, and blood **(Figure 1-6)**. GALA modification greatly enhanced lung accumulation of GALA/YSK05-MEND, while liver accumulation was largely suppressed. The Little

amount of YSK05-MEND was taken up into the lung, but it was extensively localized into the liver at 1 hour. It may be assumed that GALA modification shifts translocation of YSK05-MEND rapidly from a liver to a lung after administration. Blood retention of GALA/YSK05-MEND were shown the same time profile as lung accumulation, as they reached the peak at 1 hour and declined eventually by time. As both GALA and YSK05 function as an inducer of endosomal escape, a time-dependent decrease of GALA/YSK05-MEND in the lung might result from the constitutive activity of membrane fusion inside lung endothelial cells. This would appear to indicate that rapid endosomal destabilization of GALA/YSK05-MEND might benefit silencing activity in the lung.

### 1.5 Conclusion

The lung-targeting activity of siRNA nanocarriers was improved by the combination of GALA and a pH-sensitive lipid, YSK05. Compared to the previously-used GALA/MEND, silencing activity of GALA/YSK05-MEND in a lung increased by 3.9 fold. The accumulation of GALA/YSK05-MEND was enhanced by 11.3 fold from the unmodified YSK05-MEND. Taken together, these findings implicate the novel approach to develop effective lung-targeting siRNA nanocarriers by using GALA and YSK lipid series.

# Chapter 2

# Enhancement of lung-targeting activity of GALA by PEGylation

# Chapter 2 Enhancement of lung-targeting activity of GALA by PEGylation

## 2.1 Introduction

Previously, our laboratory unexpectedly revealed that liposomes (LPs) modified with cholesteryl-GALA (GALA/Chol-LPs) highly accumulated in lung endothelium.[19] In comparison with the GALA-unmodified liposomes, the lung accumulation of GALA-LPs was enhanced by approximately 3.5-fold within 30 minutes and retained more than 6 hours. It is commonly considered that the cationic LPs immediately form large aggregates with erythrocytes, which then rapidly accumulate in the lung. However, in this case, the lung accumulation was tentative. Thus, GALA-LPs accumulate into the lung tissue by a specific mechanism that can be distinguished from that of cationic LPs. In fact, aggregation of the LPs in the vessel was not observed in LPs when the dynamic flow of the GALA-LPs in the blood vessel was visualized by in vivo confocal laser scanning microscopy.

Incorporation of PEG into nanocarriers, termed PEGylation, has been vastly reported for improving longevity in the blood circulation.[35-37,56] PEG provides hydrophilic stealth layer as a steric barrier to reduce interaction with plasma proteins and RES uptake.[35,36,57] In addition, PEG has been widely used as a linker for ligand conjugation.[58-60] Ligand functionalization at the distal end of PEG allows improved active targeting and efficient cellular internalization of the ligand-modified nanocarriers both in vitro and in vivo.[14,61,62] For example, Maruyama et al. examined *in vivo* targeting activity of PEG-LPs terminally conjugated with the monoclonal antibody (mAb) that is highly specific to the lung endothelial cells.[63] Lung accumulation of the liposomes increased when mAb was conjugated at the end of PEG chain in comparison with that of the liposomes which mAb was directly attached to the surface.

In our laboratory, GALA was conjugated with cholesterol so that it could be directly inserted upon the nanocarrier surface. Therefore, I hypothesized that lung accumulation might be enhanced if PEG was used as a flexible linker for GALA **(Figure 2-1)**. In this part, PEGylated GALA (GALA/PEG) was synthesized and evaluated for lung accumulation.

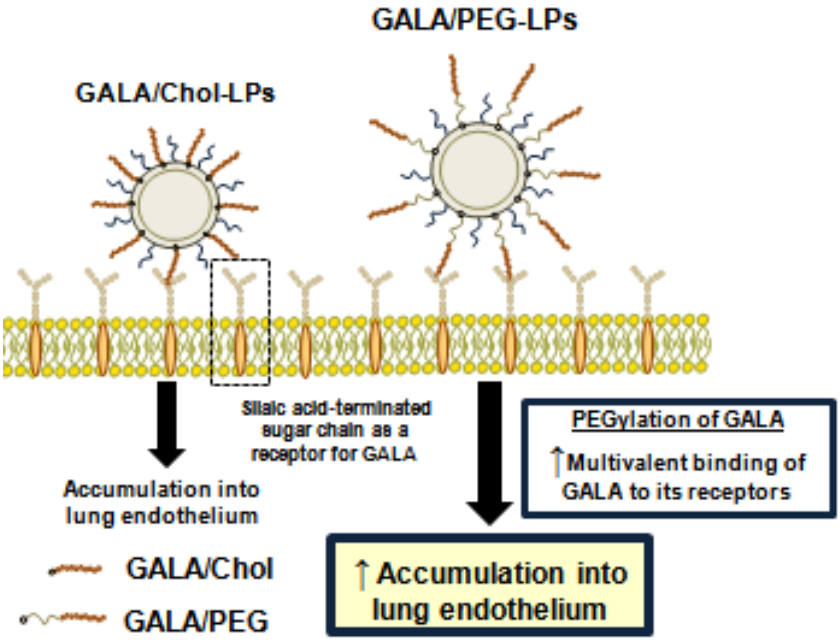


**Figure 2-1** Rationale concept of PEGylated GALA-modified LPs (GALA/PEG-LPs)

## 2.2 Materials and methods

### 2.2.1 Materials

The GALA peptide (WEAALAEALAEALAEHLAEALAEALEALAA) was purchased from PolyPeptide Laboratories SanDiego (San Diego, CA, USA). and N-(7-nitrobenz-2-oxa-1,3-diazol-4-YL)-dioleoyl-phosphatidyl-ethanolamine (NBD-DOPE) and cholesterol were purchased from AVANTI Polar Lipids (Alabaster, AL, USA). 1,2-Dimyristoyl-sn-glycerol, methoxy polyethylene glycol 2000 ether (DMG-$PEG_{2000}$), 1,2-distearoyl-sn-glycero-N-[maleimide(polyethyleneglycol)-2000] (DSG-$PEG_{2000}$-MAL), egg phosphatidylcholine (EPC) and ssPalmE were supplied from NOF Corporation (Tokyo, Japan). Stearyl-polyethyleneglycol 2000 (STR-$PEG_{2000}$) was purchased from Wako Pure Chemicals (Osaka, Japan). Endothelial basal medium-2 (EBM-2) and the EGM-2 MV SingleQuot Kit were purchased from Lonza Japan (Tokyo, Japan). 1,1'-Dioctadecyl-3,3,3',3'-tetramethyl indocarbocyanine perchlorate (DiI) was purchased from Life Technologies (Carlsbad, CA, USA). Sinapic acid and Triton™X-100 for molecular biology were purchased from Sigma-Aldrich (St.Louis, MO, USA). *Fluorescein Griffonia* (Bandeiraea) Simplicifolia Lectin I-isolectin B4 was purchased from Vector Laboratories, Inc. (Burlingame, CA, USA). 2-[4-(2-Hydroxyethyl)-1-piperazinyl]ethanesulfonic acid (HEPES) was purchased from Dojindo Laboratories (Kumamoto, Japan).

### 2.2.2 Cell Culture

Human lung microvascular endothelial cells (HMVEC-L) cells were maintained in EBM-2 containing EGM-2 MV SingleQuot Kit. The cells were cultured under an atmosphere of 5% $CO_2$/air at 37 $^{\circ}$C.

### 2.2.3 Experimental Animals

C57BL/6N mice (C57BL/6NCrSlc), 6-week old male were obtained from Sankyo Laboratories (Sapporo, Japan). The experimental protocols were reviewed and approved by the Hokkaido University Animal Care Committee in accordance with the guidelines for the care and use of laboratory animals.

### 2.2.4 Synthesis of GALA/$PEG_{2000}$

Cysteine-terminated GALA (Cys-GALA) and DSG-$PEG_{2000}$-MAL was dissolved in ethanol at concentrations of 3 mM, and then mixed at a molar ratio of 1:1. The reaction was carried under shaking at 900 rpm, 30 $^{o}$C for 24 hours. The molecular weight of Cys-GALA, DSG-$PEG_{2000}$-MAL and the reaction product was determined by Matrix-assisted laser desorption/ionization mass spectrometry (MALDI-TOF/MS). The aqueous solution of 30% acetonitrile, containing trifluoroacetic acid (0.1% v/v) and sinapic acid (1% w/v), was used as the matrix solution. The ethanol solution of GALA/$PEG_{2000}$ was kept as an aliquot of 200 µL at -20 $^{o}$C until use.

### 2.2.5 Preparation of Liposomes for *in vitro* Cellular Uptake

GALA/Chol modified liposomes (GALA/Chol-LPs), and GALA/$PEG_{2000}$ modified liposomes (GALA/$PEG_{2000}$-LPs) were prepared by the hydration method. The lipid mixture, consisting of EPC and cholesterol at a molar ratio of 7:3 plus 5 mol% of STR-$PEG_{2000}$ in a chloroform/ethanol (1:1) solution was evaporated. The dried lipid was then hydrated in HEPES buffer (pH 7.4; 10 mM) to obtain a lipid concentration of 0.55 mM. The hydrated lipid film was sonicated for approximately 1 minute in a bath-type sonicator (AU-25 C; Aiwa, Tokyo, Japan), and then for an additional 10 minutes in a probe sonicator (Branson Digital sonifier S-250D; Emerson, Connecticut, USA). For the GALA modification, 2 mol% of GALA/Chol or GALA/$PEG_{2000}$ was added to a lipid mixture of GALA/Chol-LPs or GALA/$PEG_{2000}$-LPs, respectively. 2 mol% of NBD-DOPE was also incorporated into the lipid composition to label the liposomes. The average diameter and the ζ-potential of the liposomes were determined with an electrophoretic light-scanning spectrophotometer (Zetasizer; Malvern Instrument, Worchestershire, UK).

### 2.2.6 Preparation of Liposomes for *in vivo* Observation using Confocal Microscopy

Three types of liposomes, PEGylated liposomes (PEG-LPs), GALA/Chol-LPs and GALA/$PEG_{2000}$-LPs were prepared by the hydration method. The lipid mixtures composed of EPC and cholesterol with a molar ratio of 7:3 plus 5 mol% of STR-$PEG_{2000}$ in a chloroform/ethanol (1:1 by volume) solution were evaporated. The dried lipid film was then hydrated in HEPES buffer (pH 7.4; 10 mM) containing glucose (5% w/v) to obtain a lipid

concentration of 2.64 mM. The hydrated lipid film was sonicated for approximately 1 min in a bath-type sonicator (AU-25 C; Aiwa, Tokyo, Japan), and then for an additional 10 minutes in a probe sonicator (Branson Digital sonifier S-250D; Emerson, Connecticut, USA). For the GALA modification, 2 mol% of GALA/Chol or GALA/$PEG_{2000}$ was added to the lipid mixture to form GALA/Chol-LPs or GALA/$PEG_{2000}$-LPs, respectively. 1 mol% of DiI was also incorporated into the lipid composition to label the liposomes. The average diameter and ζ-potential of the liposomes were determined using an electrophoretic light-scanning spectrophotometer (Zetasizer; Malvern Instrument, Worchestershire, UK).

**2.2.7 *In vitro* Flow Cytometry**

NBD-labeled liposomes equivalent to 55 nmole of total lipids were incubated with 2 × $10^5$ cells of HMVEC-L seeded on a six-well culture dish in the serum-free Krebs-Henseleit buffer for 1 hour at 37 °C. For flow cytometry analyses, the cells were washed three times with PBS (−). The cells were trypsinized by treatment with trypsin solution (0.05% w/v) and then suspended in EBM-2 including EGM-2 MV SingleQuot Kit.

After that, the cells were isolated by centrifugation (700 g, 4°C, 5 minutes) and washed with 1 mL of FACS buffer (PBS (−) containing bovine serum albumin (0.5% w/v) and $NaN_3$ (0.1% w/v)). After the resuspension in 0.5 mL of FACS buffer, the cell suspension was filtered through a nylon mesh to remove cell aggregates and dust. The cells were analyzed by flow cytometry (FACScan, Becton Dickinson, Franklin Lakes, NJ, USA). The cellular uptake of the liposomes is reported as the mean fluorescence intensity (MFI), which was calculated using CellQuest software (Becton Dickinson, Franklin Lakes, NJ, USA).

**2.2.8 *In vivo* Observation using Confocal Microscopy**

Lung accumulation of liposomes was evaluated at 1 hour and 6 hours after i.v. administration. DiI-labeled liposomes were injected into 6-week-old male C57BL/6N mice via the tail vein. The doses of liposomes were fixed at 26.4 μmole of lipid/kg body weight. At 30 minutes or 1 hour of post-injection, mice were sacrificed. The lungs were then reperfused using PBS(-) supplemented with heparin solution (40 units/mL). Lung samples were sliced and stained endothelium with 50 μg/mL Fluorescein *Griffonia* (Bandeiraea) *Simplicifolia*

Lectin I-isolectin B4 solution in HEPES buffer (pH 7.4; 10 mM). Lung slices were visualized by confocal laser scanning microscopy (Nikon A1; Nikon Co, Ltd., Tokyo, Japan).

## 2.3 Results

### 2.3.1 Synthesis of GALA/PEG$_{2000}$

GALA/PEG$_{2000}$ was prepared by conjugating cysteine-terminated GALA **(Cys-GALA; Figure 2-2A)** with DSG-PEG$_{2000}$-MAL **(Figure 2-2B)** via Micheal reaction in ethanol (**Figure 2-3)**.[64] The conjugation was then confirmed by MALDI-TOF MS. The mass peak (m/z) was shifted 3095.602 of DSG-PEG$_{2000}$-MAL **(Figure 2-2B)** to 6201.817 after GALA conjugation **(Figure 2-4)**. Since the change in the average molecular weight is comparable to that of Cys-GALA, that confirms that the GALA/PEG$_{2000}$ was successfully synthesized.

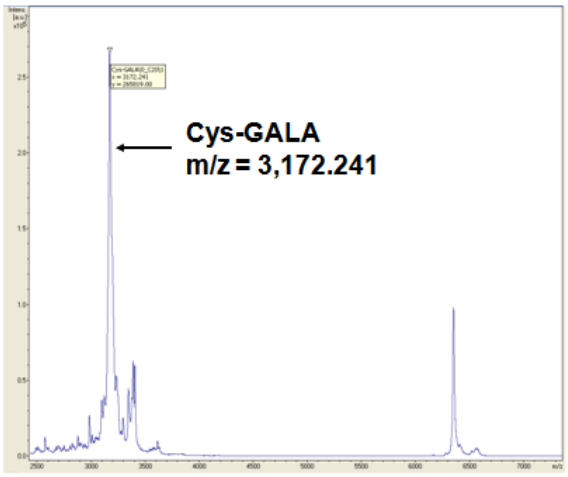


(A)

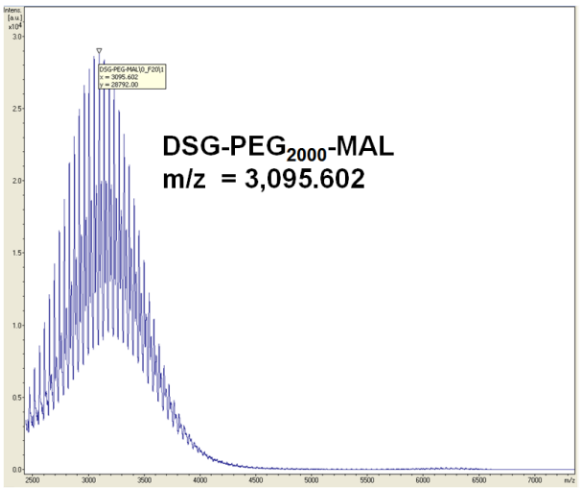


(B)

**Figure 2-2** MALDI-TOF MS spectra of (A) Cys-GALA and (B) DSG-PEG$_{2000}$-MAL

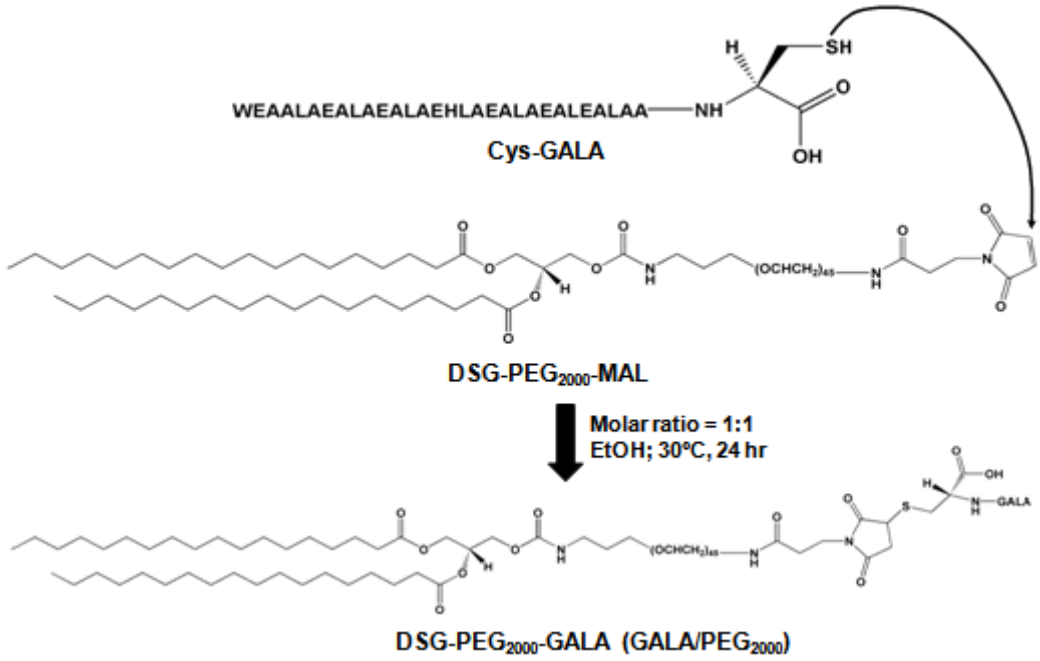


**Figure 2-3** A schematic illustration represents synthesis of GALA/$PEG_{2000}$

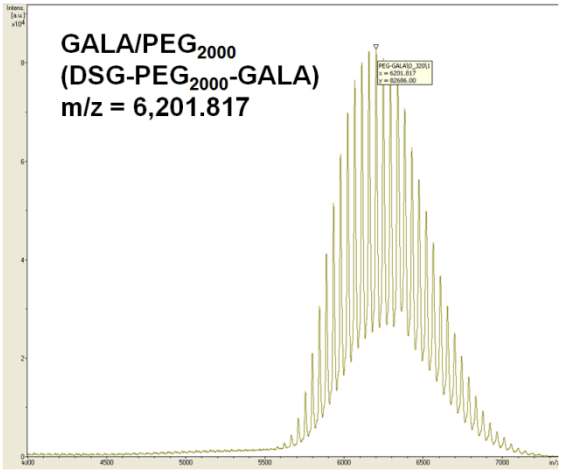


**Figure 2-4** MALDI-TOF MS spectra of GALA/$PEG_{2000}$

### 2.3.2 *In vitro* cellular uptake of GALA-modified liposomes

To examine the promoting effect of PEG linker on the GALA function toward cellular uptake, the liposomes composed of EPC and cholesterol at the molar ratio of 7:3 were prepared with pre-modification of GALA/Chol or GALA/$PEG_{2000}$ at a various amount to form GALA/Chol-LPs or GALA/$PEG_{2000}$-LPs, respectively. As a control, GALA-unmodified liposomes showed almost none of cellular uptake. At 1 mole%, GALA/Chol-LPs showed higher uptake than GALA/$PEG_{2000}$-LPs. GALA/Chol-LPs reached the uptake plateau at 2 mole% and seemed to reduce at 5 mole%. However, the uptake of GALA/$PEG_{2000}$-LPs was

superior to that of GALA/Chol-LPs at 2 mole% and reached the maximum at 5 mole%, while the excess incorporation of GALA/$PEG_{2000}$ rather than 5 mole% inversely resulted in declined cellular uptake **(Figure 2-5)**. It is suggested that PEGylated GALA enhanced the internalization of the liposomes into the lung endothelial cells.

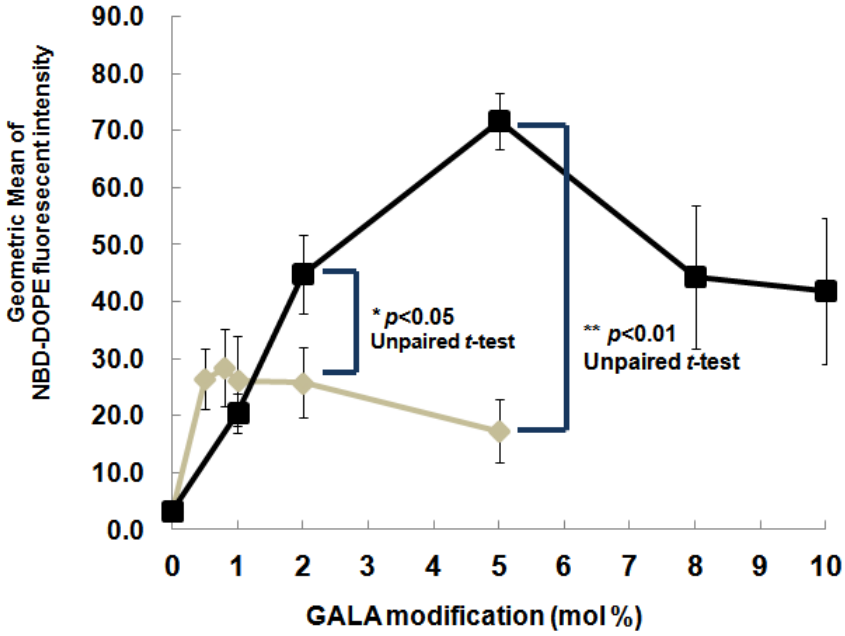


**Figure 2-5** *In vitro* cellular uptake of GALA/LPs in human lung endothelial cell. Data were represented as mean ± SD (n=3. * $p<0.05$ compared to 2 mole% GALA/Chol-LPs; ** $p<0.01$ compared to 5 mole% GALA/Chol-LPs by unpaired t-test

### 2.3.3 Preparation of GALA-modified liposomes

PEG-LPs composed EPC and cholesterol at the molar ratio of 7:3 plus 5 mole% of STR-$PEG_{2000}$ as a vesicle stabilizer were prepared. To modify the liposome surface by GALA, 2 mole% of GALA/Chol or GALA/$PEG_{2000}$ was incorporated into the lipid composition before evaporating organic solvent, then forming GALA/Chol-LPs or GALA/$PEG_{2000}$-LPs, respectively. The liposomes were further labeled with 1 mole% of the fluorescent marker, DiI. As shown in **Table 2-1**, PEG-LPs were slightly larger than GALA-modified LPs. However, GALA-modified LPs (< -20 mV) became more negatively-charged than PEG-LPs (approximately 3 mV). Also, the zeta potential of GALA/$PEG_{2000}$-LPs was slightly lower than that of GALA/Chol-LPs.

**Table 2-1** Physicochemical characteristics of PEG-LPs, GALA/Chol-LPs and GALA/$PEG_{2000}$-LPs (mean ± SD; n=3-4)

| Liposomes | Size (nm) | PDI | Zeta potential (mV) |
|---|---|---|---|
| **PEGylated** | 98 ± 13 | 0.21 ± 0.03 | -2.8 ± 2.9 |
| **GALA/Chol** | 85 ± 7 | 0.26 ± 0.02 | -23.4 ± 2.5 |
| **GALA/$PEG_{2000}$** | 82 ± 14 | 0.18 ± 0.03 | -28.3 ± 4.1 |

### 2.3.3 Effect of PEGylation on lung accumulation of GALA-modified liposomes

To investigate the effect of a PEG spacer on the function of GALA as a ligand targeting lung endothelium, the accumulation of DiI-labeled liposomes (PEG-LPs, GALA/Chol-LPs, and GALA/$PEG_{2000}$-LPs) was observed via confocal microscopy at 30 minutes, 1 and 6 hours of post-injection.

At 30 minutes, little amount of PEG-LPs were found in the lung endothelium **(Figure 2-6(a)),** while GALA/Chol-LPs accumulated along with the vessel structure **(Figure 2-6(b))**. Most importantly, GALA/$PEG_{2000}$-LPs were rapidly accumulated in the lung endothelium to the greater extent than GALA/Chol-LPs **(Figure 2-6(c))**. The fluorescence gradually decreased in all of the LPs at 1 hour **(Figure 2-7(a-c))** and further at 6 hours **(Figure 2-8(a-c))**. From these results, it was suggested that the topology of the GALA in the surface of the liposomes drastically affect the lung targeting efficacy of GALA.

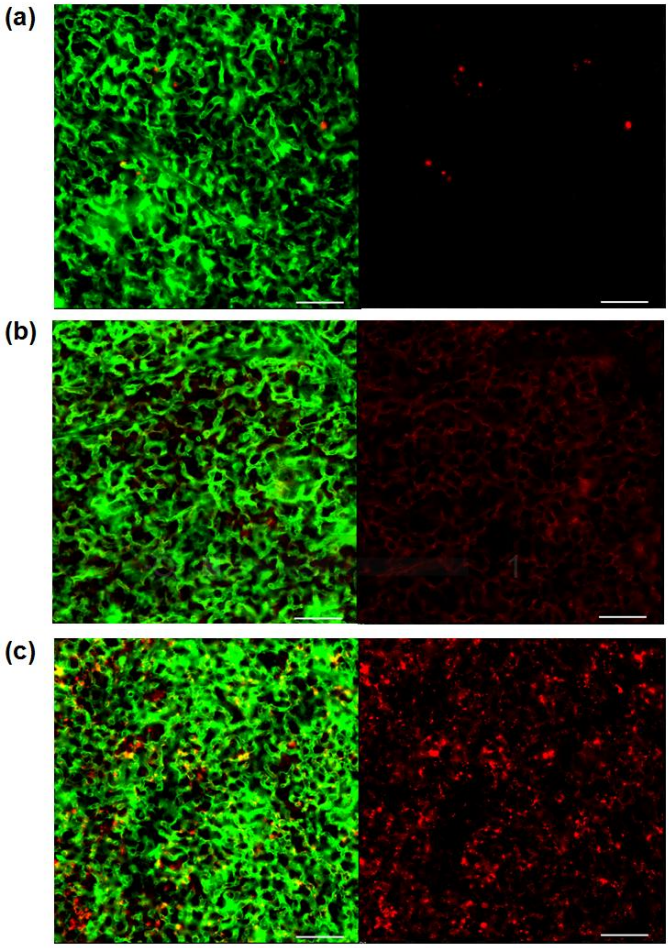


**Figure 2-6** Lung accumulation of (A) PEG-LPs, (B) GALA/Chol-LPs and (C) GALA/$PEG_{2000}$-LPs at 30 minutes after liposome injection

C57BL/6N mice (6-week, male) were injected with DiI-labeled PEG-LPs, GALA/Chol-LPs and GALA/$PEG_{2000}$-LPs at 26.4 μmole lipid/kg dose. At 30 minutes after injection, the lung was perfused with heparin solution in PBS(-) and sliced for endothelial staining with FITC-isolectin B4. All slices were observed via confocal microscopy. Scale = 50 μm.

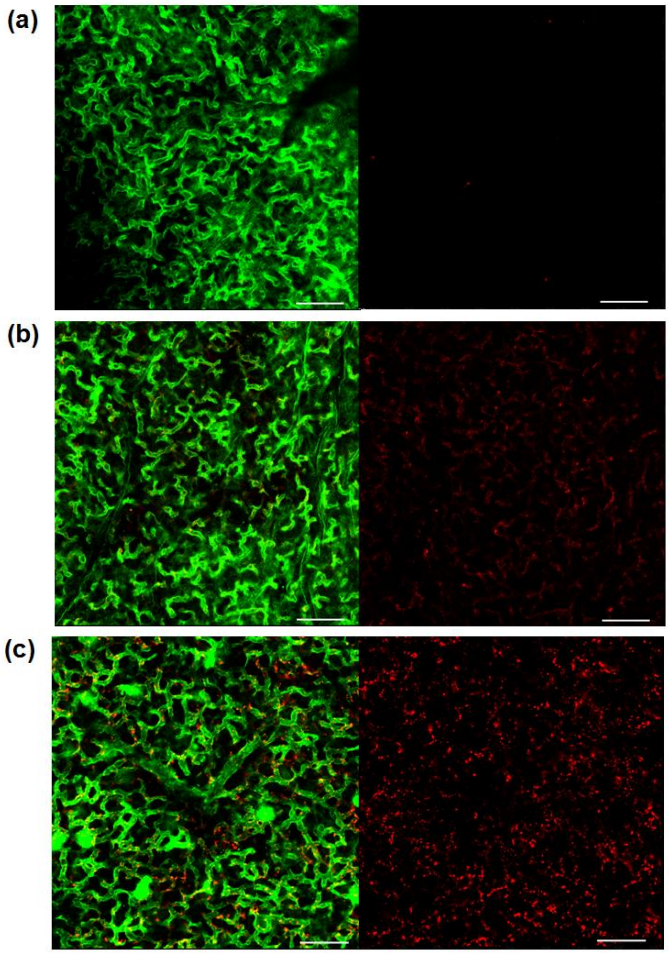


**Figure 2-7** Lung accumulation of (A) PEG-LPs, (B) GALA/Chol-LPs and (C) GALA/$PEG_{2000}$-LPs at 1 hour after liposome injection

C57BL/6N mice (6-week, male) were injected with DiI-labeled PEG-LPs, GALA/Chol-LPs and GALA/$PEG_{2000}$-LPs at 26.4 μmole lipid/kg dose. At 1 hour after injection, the lung was perfused with heparin solution in PBS(-) and sliced for endothelial staining with FITC-isolectin B4. All slices were observed via confocal microscopy. Scale = 50 μm.

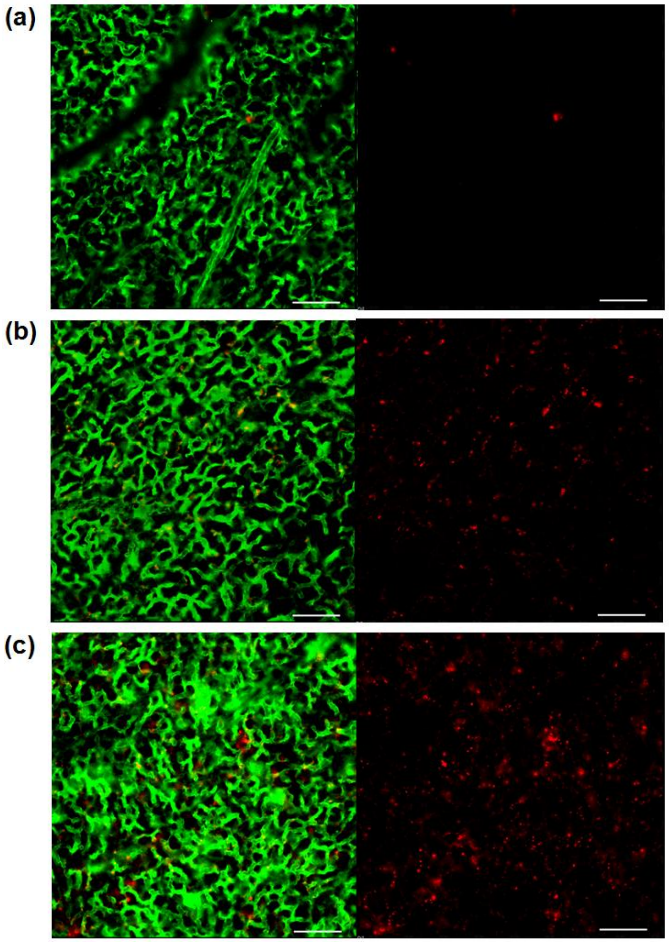


**Figure 2-8** Lung accumulation of (A) PEG-LPs, (B) GALA/Chol-LPs and (C) GALA/$PEG_{2000}$-LPs at 6 hours after liposome injection

C57BL/6N mice (6-week, male) were injected with DiI-labeled PEG-LPs, GALA/Chol-LPs and GALA/$PEG_{2000}$-LPs at 26.4 μmole lipid/kg dose. At 6 hours after injection, lung was perfused with heparin solution in PBS(-) and sliced for endothelial staining with FITC-isolectin B4. All slices were observed via confocal microscopy. Scale = 50 μm.

**2.4 Discussion**

As well as the function of GALA as an inducer of endosomal escape, GALA also functions as a targeting ligand for lung endothelium.[19] The previous study revealed that lung accumulation of the immune-liposomes using lung endothelium-specific mAb as targeting ligand was increased when mAbs were attached to the distal end of PEG.[63] We have also revealed that modification of transferrin [65] on the PEG terminal improved receptor-ligand internalization of Tf-modified liposomes (Tf-L).[14,66] Similarly, surface display of GALA using PEG polymer as spacer increased cellular uptake to the lung endothelium-derived cells (HMVEC-L) of the nanocarriers **(Figure 2-5)**.

The zeta potential of both GALA/Chol-LPs and GALA/$PEG_{2000}$-LPs was lower than -20 mV, while the corresponding value in PEG-LPs was neutral **(Table 2-1)**. It is reasonable since GALA contains 7 residues of negatively-charged amino acids (glutamic acids) in its peptide.[13]

Lung accumulation of both liposomes was observed via confocal microscopy **(Figure 2-6 to 2-8)**. As a result, GALA/$PEG_{2000}$-LPs accumulated in the lung endothelium rapidly at the first 30 minutes to a higher degree than GALA/Chol-LPs. From these results, it was suggested that PEG linkers might influence the binding activity of GALA toward sugar receptors on the lung endothelial cells.

The effect of flexible PEG spacers on binding affinity on target receptors was previously investigated. Frisch B et al. evaluated target accessibility of the trigalactosyl ligand conjugated at the terminal of PEG chain.[67] The lipoplexes containing the PEGylated trigalactosyl scaffolds showed a positive test for ricin agglutination at the low charge ratio of cationic lipid/pDNA, whereas the lipoplexes containing the non-PEGylated ones formed aggregates only at the higher charge ratio. Thus, ligand became more accessible by ligand conjugation at terminal side of PEG chain.[67,68]

In another report, Paranjpe et al. showed *in vitro* cytotoxicity of the glycine-camptothecin conjugate (CPT-Gly) against KB cells that typically overexpress in folate receptors. CPT-Gly, in that folate, was conjugated to the PEG spacer (CPT-Gly-PEG-folate) obtained the highest antitumor activity among the CPT-Gly in that folate was directly

conjugated (CPT-Gly-folate), or the PEGylated one without folate modification (CPT-Gly-PEG). The group further performed molecular docking of CPT-Gly-folate and CPT-Gly-PEG-folate to measure spacer length. The length of glycine spacer was 3.7 Å, whereas the length of the glycine-PEG spacer was 195 Å. Therefore, the ligand that can more freely move can gain access to the receptor expressed on the cell membrane.[69] Alternatively, the ligand that was displayed on the longer PEG can more readily associate with the receptor that is located far from the liposomes and allow the liposomes to anchor to the cells via multivalent ligand-to-receptor binding. As an advantage, the strong binding could be achieved with modest or low surface area. In addition, the stronger interaction could be collectively evolved with increasing the number of weak individual interactions. As a model, influenza viruses attaches to bronchial epithelial cells by using trimeric hemagglutination to simultaneously recognize multiple moieties of sialic acid on the target cell surfaces, which promotes endocytosis and leads to infection.[70] Thus, it is the most plausible that hydrophilic and flexible PEG chain assisted GALA to approach its pattern of sialic acid-terminated sugar chains on the endothelial cell surface.

**2.5 Conclusion**

Binding activity of GALA as target ligand for lung endothelium was improved when it was conjugated onto the PEG spacer, in comparison with that modified directly onto the liposome surface. GALA/$PEG_{2000}$-LPs were taken up rapidly and extensively in the lung endothelium *in vitro* and *in vivo*. It is the most plausible that the GALA modified on the liposomes with high flexibility can bind to the sialic acid-terminated sugar chains on lung endothelium.

# Chapter 3

# Cellular trafficking of GALA

# Chapter 3 Cellular trafficking of GALA

## 3.1 Introduction

GALA is designed to mimic a structure of influenza viral protein, hemagglutinin (HA) which promotes internalization and endosome fusion.[13] Before entry, HA recognizes and binds sialic acid which is a cell surface receptor.[71,72] Sialic acid is typically attached to the underlying galactose by α-2,3 or α-2,6 linkages which influence surface binding. According to the previous report[19], cellular uptake of GALA-LPs was strongly inhibited by *Maackia amurenesis* Agglutinin (MAM) and *Sambucus sieboldiana* Agglutinin which have an affinity for two lectin subtypes; SAα2,3Gal and SAα2,6Gal, respectively. However, sialic acid did not directly inhibit the liposome uptake. Likewise, unlike influenza virus, GALA-LPs do not recognize terminal sialic acid on the surface receptor. Instead, they recognize sialic acid-containing sugar patterns before internalization.

There are more questions regarding cellular trafficking of GALA. First, uptake mechanism remains poorly understood. Endocytosis of GALA-modified nanocarriers was confirmed since the cell uptake was suppressed at 4ºC.[73] Nevertheless, an endocytosis pathway has never been investigated. Second, according to Part 2, extravasation of GALA-LPs was presented in confocal images (White circles in **Figure 3-1**). GALA-modified nanocarriers were supposed to have transendothelial activity so that they could reach other lung tissues such as alveolar epithelium. Similarly, GALA might possess an ability to initiate endothelial transcytosis.

In this part, the study was aimed at two objectives; (1) to clarify an entry route of GALA-modified nanocarriers, and (2) to evaluate transcytosis activity of GALA. An endocytosis pathway was examined *in vitro* by an inhibitory assay using pharmacological inhibitors, and a confocal observation using endocytosis markers.

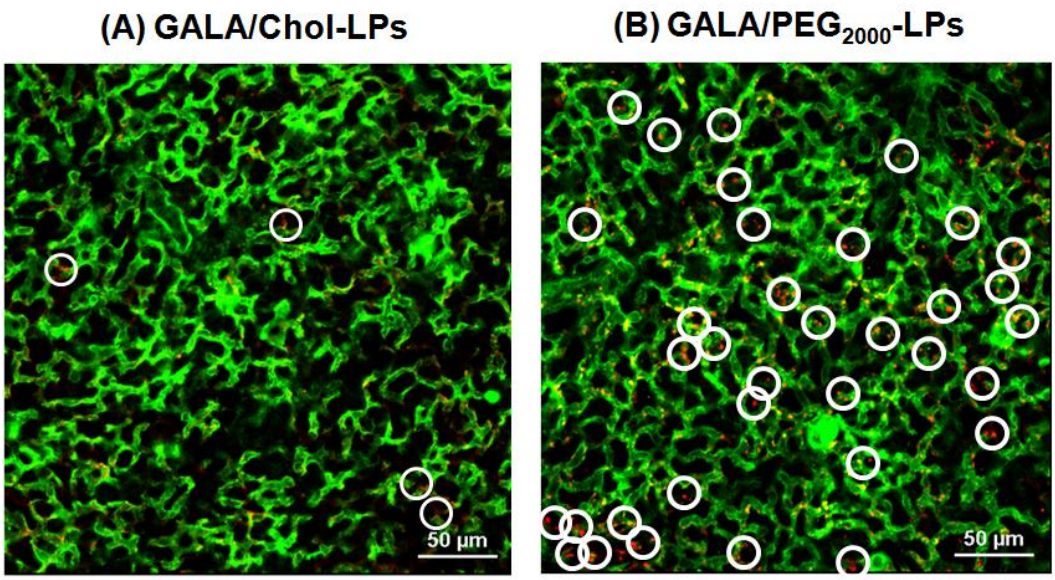


**Figure 3-1** Confocal images depict extravasation of GALA/Chol-LPs (A) and GALA/$PEG_{2000}$-LPs (B) in the lung. Green represents blood vessels, whereas red represents liposomes. Extravasated liposomes were marked in white circles. Scale: 50 μm

Meanwhile, transcytosis was investigated *in vivo* with three experiments. First, accumulation of GALA-modified nanocarriers was quantified in both lung endothelium and Type I alveolar epithelium by flow cytometry. Second, silencing activity of GALA/MEND were evaluated in Type I alveolar epithelium. Finally, localization of GALA/MEND encapsulating gold nanoparticles (GALA/MEND-AuNPs) were observed in lung tissues by transmission electron microscopy (TEM). It was hypothesized that, if GALA possesses an intrinsic activity for transcytosis, GALA-modified nanocarriers would penetrate lung endothelium and be taken up in other tissues such as alveolar epithelium **(Figure 3-2)**.

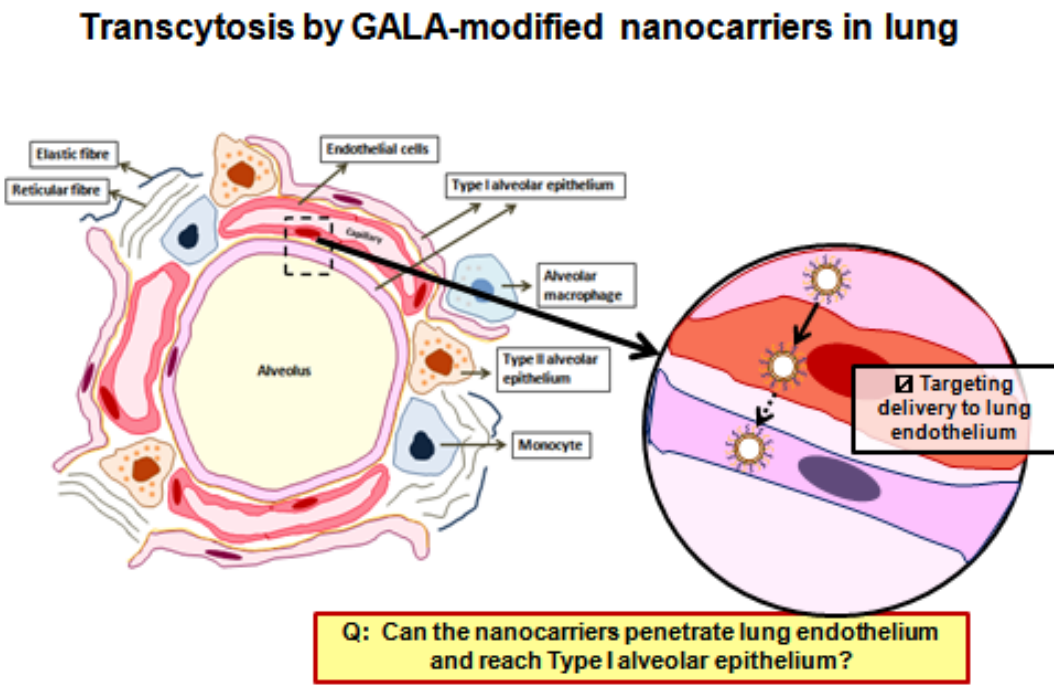


**Figure 3-2** Graphical illustration shows the hypothesis of transcytosis activity by GALA-modified nanocarriers.

### 3.2 Materials and Methods

#### 3.2.1 Materials

Anti-Pdpn siRNAs were purchased from Hokkaido System Science Co., Ltd. (Sapporo, Japan). Primers and probes for Podoplanin (Pdpn) and GADPH were ordered from Sigma-Aldrich (St. Louis, MO, USA). Sequence information was listed in section 3.2.2. GALA peptide (WEAALAEALAEALAEHLAEALAEALEALAA) was purchased from PolyPeptide Laboratories (San Diego, CA, USA). Egg phosphatidylcholine and Cholesterol was ordered from AVANTI Polar Lipids (Alabaster, AL, USA). Stearyl-polyethylene glycol 2000 (STR-$PEG_{2000}$),

1,1'-dioctadecyl-3,3,3',3'-tetramethylindodicarbocyanine, 4-chlorobenzene sulfonate salt (DiD) and 1,1'-dioctadecyl-3,3,3',3'-tetramethylindocarbocyanine-5,5'-disulfonic acid (DiI) were ordered from Thermo Fisher Scientific, Inc. (Waltham, MA, USA). 2-[4-(2-Hydroxyethyl)-1-piperazinyl]ethanesulfonic acid (HEPES) was purchased from Dojindo Laboratories (Kumamoto, Japan). Trizol® Reagent and Quant-iT™ RiboGreen assay were purchased from Thermo Fisher Scientific, Inc. (Waltham, MA, USA). Thunderbird™ SYBR® qPCR Mix and ReverTra Ace® qPCR RT Master Mix with gDNA Remover was purchased from Toyobo Co., Ltd. (Osaka, Japan). PELCO® NanoXactTM 5 nm 5 Cap Gold was purchased from TED PELLA, Inc. (Redding, CA, USA).

EGM™-2MV BulleKit™ medium was purchased from Lonza, Ltd. (Basel, Switzerland). Hank's balanced salt solution (HBSS) and Purified normal mouse serum IgG (Whole Molecule) were was purchased from Wako Pure Chemicals (Osaka, Japan). Alexa Fluor® 488-conjugated Dextran (MW=10,000), Alexa Fluor® 488-conjugated Cholera Toxin Subunit B (Recombinant; CTB) and Alexa Fluor® 647-conjugated Transferrin From Human Serum were purchased from Thermo Fisher Scientific, Inc. (Waltham, MA, USA). Filipin III from *Streptomyces filipinensis*, chlorpromazine hydrochloride, and amiloride hydrochloride hydrate was purchased from Sigma-Aldrich, Co., LLC. (St.Louis, Missouri, USA). Hoechst 33342 and 2-[4-(2-Hydroxyethyl)-1-piperazinyl]ethanesulfonic acid (HEPES) were obtained from Dojindo Laboratories (Kumamoto, Japan). RPMI-1640 medium, 1 M HEPES buffer,

RBC lysis buffer and Triton X-100 was purchased from Sigma-Aldrich (St. Louis, MO, USA). Glycogen (M.B.) was acquired from GMbiolab Co., Ltd. (Taichung, Taiwan).

Type I collagenase and crystallized elastase from porcine pancreas (High purity) was purchased from EMD Millipore Corp. (Billerica, MA, USA). DNase I from bovine pancreas was ordered from Worthington Biochemical Corp. (Lakewood, NJ, USA). Purified anti-mouse CD16/CD32 antibody (Clone: 2.4G2) and FITC anti-mouse CD45 antibody (Clone: 30-F11) were ordered from Tonbo Biosciences (San Diego, CA, USA). FITC anti-mouse CD31 antibody (Clone: 390), PE anti-mouse CD31 (Clone: 390), PE anti-mouse Podoplanin antibody (Clone: 8.1.1) and PE-Cy7 EpCAM (CD326) antibody (Clone: G8.8) were purchased from Biolegend (San Diego, CA, USA). FITC Rat IgG 2b, κ isotype control, FITC Rat IgG 2a, κ isotype control, PE Syrian hamster IgG isotype control and PE/Cy7 Rat IgG 2a, κ isotype control were purchased from Biolegend (San Diego, CA, USA). PE Rat IgG 2a, κ isotype control was purchased from BD Biosciences (San Jose, CA, USA).

### 3.2.2 siRNA and primer sequences

#### siRNA

Pdpn-targeting siRNAs were ordered from Hokkaido Bioscience Systems (Hokkaido, Japan). The siRNAs included the mixture from 4 sequences as shown in **Table 3-1**.

**Table 3-1** Sequences of Pdpn-targeting siRNAs

| siRNA name | Sequences (5'→3') | Molecular weight (g/mole) | Length | Tm (°C) |
|---|---|---|---|---|
| Pdpn1 | Sense: AAUCAUAGUUGGCGUCUUG(dTdT) | 6647.9 | 21 | 47.2 |
| | Antisense: CAAGACGCCAACUAUGAUU(dTdT) | 6637.0 | 21 | 47.2 |
| Pdpn2 | Sense: GAGCUAAACAGAACAGGUU(dTdT) | 6740.0 | 21 | 42.8 |
| | Antisense: AACCUGUUCUGUUUAGCUC(dTdT) | 6544.8 | 21 | 42.8 |
| Pdpn3 | Sense: GGACUAUAGGCGUGAAUGA(dTdT) | 6773.0 | 21 | 47.0 |
| | Antisense: UCAUUCACGCCUAUAGUCC(dTdT) | 6526.8 | 21 | 47.0 |
| Pdpn4 | Sense: UGUAAAGGUUUGCGGUUAA(dTdT) | 6711.9 | 21 | 48.3 |
| | Antisense: UUAACCGCAAACCUUUACA(dTdT) | 6557.9 | 21 | 48.3 |

**Primers**

Primers for Pdpn and GAPDH were ordered from Sigma-Aldrich (St. Louis, MO, USA). Sequences were shown in **Table 3-2**.

**Table 3-2** Sequences of Pdpn- and GADPH-targeting primers

| Primer name | Sequences (5'→3') | Molecular weight (g/mole) | Length | Tm (ºC) |
|---|---|---|---|---|
| Mm_podoplanin-F | CCCAATAGAGATGGCTTGCCAG | 6744.5 | 22 | 68.6 |
| Mm_podoplanin-R | GCGAGAACCTTCCAGAAATCTTC | 6992.6 | 23 | 66.0 |
| GAPDH F1 | AGCAAGGACACTGAGCAAG | 5879.9 | 20 | 60.8 |
| GAPDH R1 | TAGGCCCCTCCTGTTATTATG | 6363.2 | 20 | 61.6 |

### 3.2.3 Cells

Human lung microvascular endothelial cells (HMVEC-L; Lonza, USA) were cultured with EGM$^{TM}$-2MV BulleKit$^{TM}$ medium (Lonza, USA) at 37$^{0}$C, 5% $CO_2$. Cells between passage 2-8 were used for experiments.

### 3.2.4 Mice

Male C57BL6/J mice (6-8 weeks, 20-25 grams) were from Nihon Clea Co., Ltd. (Tokyo, Japan).

### 3.2.5 WST8-assay

$5x10^3$ cells of HMVEC-L were seeded in a 96-well plate and grown to 80-90% confluency for 24 hours. For inhibitor treatment, filipin III, amiloride in DMSO and chlorpromazine in the aqueous solution was diluted in 10 µL/well of serum-lack EBM to reach the certain concentration. The cells were co-incubated with the inhibitor at 3 hours and 30 minutes. The cck-2 reagent was then added by 10 µL/well, and the incubation continued for 2 hours. Finally, the absorbance was measured at $\lambda_{max}$ of 450 nm by the plate reader (EnSpire 2300 multilabel reader; Perkin Elmer, Waltham, MA, USA).

### 3.2.6 Liposome preparation for *in vitro* studies

EPC and cholesterol in ethanol were added to the glass tube at the molar ratio of 7:3. 5 mole% of STR-mPEG$_{2000}$ and 2 mole% of GALA/Chol were added for modification. 0.3 mole% DiD or 1 mole% DiI was then added to label the lipid. Chloroform was added to the lipid mixture to make the final lipid concentration of 550 µM.

The lipid solution was evaporated with a vacuum desiccator to form a thin film. 800 µL of HEPES buffer (pH 7.4; 10 mM) was added and left for 15 minutes at the room temperature. The tube was sonicated with a bath sonicator and further with a probe sonicator for a minute and 10 minutes, respectively. After that, the liposomes were transferred into an Eppendorf tube and centrifuged twice at 15000 rpm, 20°C, 5 minutes. The liposomes were finally stored at $4^0$C until use.

### 3.2.7 *In vitro* cellular uptake study

$4x10^4$ cells of HMVEC-L were seeded in a 24-well plate and grown to 80-90% confluency for 24 hours. Media was aspirated, and the cells were washed with Hank's balanced salt solution (HBSS). The cells were co-incubated with the DiD-labeled GALA/Chol-LPs (11 nmole lipids) in 500 µL of serum-lack endothelial basal medium (EBM-2). After 3 hour post-incubation, the cells were washed three times with PBS(-) and trypsinized. Cells were neutralized with serum-added EBM and suspended with FACS buffer for FACS analysis. A total of 10,000 events were counted in each sample with BD FACSCalibur (BD Biosciences, USA).

For inhibitor treatment, filipin III, amiloride in DMSO and chlorpromazine in the water was diluted in 1 mL serum-lack EBM to reach the certain concentration. The cells were co-incubated with the inhibitor at 30 minutes before adding the liposomes.

### 3.2.8 *In vitro* confocal observation

$2x10^5$ cells of HMVEC-L were seeded in 3.5-mm glass bead dish and grown to 80-90% confluency for 24 hours. Media was aspirated, and cells were replaced with 2 mL of Krebs- a Henseleit solution containing the following fluorescent markers; Alexa Fluor® 488-conjugated CTB (5 µg/mL), Alexa Fluor® 647-conjugated transferrin (100 µg/mL) or Alexa Fluor® 488-conjugated amiloride (500 µg/mL). Pre-incubation of the markers took 15 minutes

for dextran-treated cells, and 1 hour for CTB- and transferring-treated cells. Then, the DiI-labeled GALA/Chol-LPs (55 nmole lipids) was added. After 2 hour post-incubation, the cells were washed three times with PBS(-) and replaced with 2 mL of Krebs-Henseleit solution. Nuclei were stained with Hoechst 33342 (1 µg/mL) at 10 minutes prior to cell washing.

Cells were visualized by Nikon-A1 microscope (Nikon, Japan) with a 60x water lens (Plan Apo Vc 60x WI DIC N2).

### 3.2.9 Synthesis of GALA/$PEG_{2000}$

Cysteine-terminated GALA (Cys-GALA) and DSG-$PEG_{2000}$-MAL was dissolved in 99% EtOH at concentrations of 3 mM and mixed at a molar ratio of 1:1. The reaction was carried under shaking at 900 rpm, 30 $^{o}$C for 24 hours. The molecular weight of Cys-GALA, DSG-$PEG_{2000}$-MAL and the reaction product was determined by MALDI-TOF/MS. The results collected from MALDI-TOF/MS were presented in Part 2. The aqueous solution of acetonitrile (30% v/v), containing TFA (0.1% v/v) and sinapic acid (1% w/v), was used as the matrix solution. The ethanol solution of GALA/$PEG_{2000}$ was kept as an aliquot of 200 µL at -20 $^{o}$C.

### 3.2.10 Synthesis of GALA/$PEG_{5000}$

Cysteine-terminated GALA (Cys-GALA) and DSPE-$PEG_{5000}$-MAL was dissolved in 99% EtOH at concentrations of 3 mM and mixed at a molar ratio of 1:1. The reaction was carried under shaking at 900 rpm, 30 $^{o}$C for 24 hours. The molecular weight of Cys-GALA, DSPE-$PEG_{5000}$-MAL and the reaction product was determined by MALDI-TOF/MS. The aqueous solution of acetonitrile (30% v/v), containing TFA (0.1% v/v) and sinapic acid (1% w/v), was used as the matrix solution. The ethanol solution of GALA/$PEG_{2000}$ was kept as an aliquot of 200 µL at -20 $^{o}$C.

### 3.2.11 Liposome preparation for *in vivo* studies

An ethanol solution of EPC and cholesterol were added to the glass tube at the 7:3 molar ratio. For PEG and GALA modification, 5 mole% of STR-$PEG_{2000}$ and 2 mole% of GALA/Chol, GALA/$PEG_{2000}$ or GALA/$PEG_{5000}$ were added to the solution. DiD was further added to 0.3 mole% to label the lipid. After that, chloroform was added to the lipid mixture to obtain the final lipid concentration of 2.64 mM.

The lipid solution was evaporated with a vacuum desiccator to form a thin film. The equivalent volume of HEPES buffer (pH 7.4; 10 mM) containing 5% glucose was added and left at the room temperature for 15 minutes. After that, the tube was sonicated in a bath-type sonicator (AU-25 C; Aiwa, Tokyo, Japan) and a probe sonicator (Branson Digital sonifier S-250D; Emerson, Connecticut, USA) for a minute and 10 minutes, respective. The pre-formed liposomes were transferred into an Eppendorf tube and centrifuged twice at 15000 rpm, 20°C, and 5 minutes.

**3.2.12 Liposome administration**

The liposomes were injected at a lipid dose of 26.4 nmol/kg body weight (equivalent to 10 µL/kg body weight) into a 6-week male C57BL/6J mouse, using the syringe with a 27G-needle (Terumo Co., Tokyo, Japan).

**3.2.13 Enzymatic digestion**

Before sacrificing mice, the following solutions were freshly prepared and kept on ice.

| | | |
|---|---|---|
| **Solution A** | 1 mL for one mouse | |
| | 0.02 mg/mL | DNase I |

The solution A was prepared in RPMI-1640 supplemented with 25 mM HEPES (RPMI-1640 – HEPES).

| | | |
|---|---|---|
| **Solution B** | 6 mL for one mouse | |
| | 4 mg/mL | Type I collagenase |
| | 4.5 U/mL | Elastase |
| | 10% (w/v) | Dextran |
| | 0.02 mg/mL | DNaseI |
| | 3 mM | $CaCl_2$ |

All components were dissolved or diluted in RPMI-1640 – HEPES.

| | | |
|---|---|---|
| **Solution C** | 20 mL for one mouse | |
| | 50% (v/v) | fetal bovine serum |

The solution C was prepared in RPMI-1640 – HEPES.

Mice were killed by $CO_2$ asphyxiation under dry ice. The stomach was opened vertically and horizontally. A diaphragm and inferior vena cava were cut to drain blood from

the systemic circulation. Ribs were cut ventrally and laterally, to expose a heart, a lung, and a trachea. Lung perfusion was done through the right ventricle by using the syringe with a 26G-needle (Terumo Co., Tokyo, Japan) and 10-15 mL of ice-cold HBSS. A 22G Surfloflash® catheter was then inserted into the trachea and tied with a pair of surgical thread. The lung was lavaged with 5 mL of EDTA solution (5 mM) in DPBS (-), followed by one mL of solution A. Next, the lung was infused with two mL of solution B and one mL of 1% low-melting-point agarose solution, and was cooled down with ice to solidify the agarose. The catheter was removed from the trachea. After that, the lung was separated from ribs by cutting the top of the trachea, surrounding tissues, and cardiac tissues. The lung was placed in the 6-well plate containing two mL/well of solution A, and incubated at 37ºC, 45 minutes in the shaking incubator.

The trachea was removed, and the lung was minced with a razor blade at 200 strokes. The minced lung was transferred to the new well which contains solution A. Incubation was repeated for more 15 minutes. The digested lung tissues were transferred into the 50-mL Falcon tube containing 20 mL of solution C. To purify alveolar epithelium and lung endothelium, mouse serum IgG was added at the final concentration of 10 µg/mL, and then incubated on ice for 10 minutes.[74,75] Incubation was repeated at room temperature for 5 minutes, 300 rpm. Cell suspensions were filtered through 100-µm nylon mesh (BD Biosciences, North Carolina, USA), and washed through the filter with two mL of DPBS (-). The suspensions were centrifuged at 2000 rpm, 4ºC for 5 minutes. Washing step was repeated with five mL of RPMI-1640 – HEPES. The cells were treated with one mL of RBC lysis buffer at room temperature for 2 minutes, and washed with five mL of solution C. Washing step was repeated with five mL of RPMI-1640 – HEPES, and was filtered 70-µm nylon mesh (BD Biosciences, North Carolina, USA). Centrifugation was repeated, and total cells were re-suspended in 5 mL of FACS buffer. Cell counting was done with the cell counter (LUNA™ Automated Cell Counter; Logos Biosystems, Inc., USA).

**3.2.14 Antibody staining**

The staining condition was modified from the method reported by Yamamoto, et al.[76] Cell suspensions were transferred at the equivalent amount of $1x10^6$ cells into the new

eppendorf tube. The cells were stained at $1x10^6$ cells/100 µL of the antibody solution, under the following condition

**Antibody staining for Type I alveolar epithelium**

| | |
|---|---|
| FITC anti-mouse CD45 antibody | 0.1 µg |
| FITC anti-mouse CD31 antibody | 0.1 µg |
| PE anti-mouse Podoplanin antibody | 0.1 µg |
| PE-Cy7 EpCAM (CD326) antibody | 0.1 µg |
| FACS buffer containing anti-mouse CD16/CD32 antibody in (40 µg/mL) | to 100 µL |

**Control staining for Type I alveolar epithelium**

| | |
|---|---|
| FITC Rat IgG 2b, κ isotype control | 0.1 µg |
| FITC Rat IgG 2a, κ isotype control | 0.1 µg |
| PE Syrian hamster IgG isotype control | 0.1 µg |
| PE/Cy7 Rat IgG 2a, κ isotype control | 0.1 µg |
| FACS buffer containing anti-mouse CD16/CD32 antibody in (40 µg/mL) | to 100 µL |

**Antibody staining for lung endothelium**

| | |
|---|---|
| FITC anti-mouse CD45 antibody | 0.1 µg |
| PE anti-mouse CD31 antibody | 0.1 µg |
| FACS buffer containing anti-mouse CD16/CD32 antibody in (40 µg/mL) | to 100 µL |

**Control staining for lung endothelium**

| | |
|---|---|
| FITC Rat IgG 2b, κ isotype control | 0.1 µg |
| PE Rat IgG 2a, κ isotype control | 0.1 µg |
| FACS buffer containing anti-mouse CD16/CD32 antibody in (40 µg/mL) | to 100 µL |

Cells were stained on ice for 30 minutes and then washed with FACS buffer. Finally, the cells were analyzed with FACS Calibur (BD Biosciences, USA).

### 3.2.15 Preparation of GALA-MEND using DOTMA

50 µL of siRNA solution (2 mg/mL) in DEPC-treated water was diluted in 250 µL of HEPES buffer (pH 7.4; 10 mM) containing glucose (5% w/v), to obtain siRNA solution with a concentration of 333 µg/mL. Meanwhile, 25 µL of 10kDa-branched polyethyleneimine solution (10kDa-bPEI; 1 mg/mL) in deionized water was diluted in 200 µL of HEPES buffer

(pH 7.4; 10 mM) containing glucose (5% w/v), to obtain the 10kDa-bPEI solution with a concentration of 125 µg/mL. siRNA cores with a N/P ratio of 1.8 were prepared, by adding the 10kDa-bPEI solution dropwise in the siRNA solution, under the moderate vortex speed. Size and zeta potential were measured with Nano-ZS Zeta Sizer (Malvern instrument, UK). siRNA cores have the negative zeta potential below -20 mV.

Lipid solution was prepared in ethanol at a total lipid concentration of 2.64 mM: DOTMA, cholesterol, EPC at 3:4:3 molar ratio plus 5 mole% of STR-$PEG_{2000}$ and 2 mole% GALA (GALA/Chol, GALA/$PEG_{2000}$, and GALA/$PEG_{5000}$). The solution was dried in the vacuum desiccators to form the lipid film. When the film was completely dried, the solution of siRNA core was added into the tube, and the film was left hydrated for 15 minutes. The tube was sonicated in the bath-type sonicator (AU-25 C; Aiwa, Tokyo, Japan), so that MEND could be formed. The MEND solution was finally transferred to the Eppendorf tube. Size and zeta potential were measured with Nano-ZS Zeta Sizer (Malvern instrument, UK).

**3.2.16 Intravenous administration of MEND**

MEND was intravenously administered at 1.5 mg/kg dose via a tail vein. At 24 hours after administration, mice were sacrificed to collect lung into the Eppendorf tubes and were frozen in the liquid nitrogen. 30-40 mg of organ tissues were sampled or as a whole for RNA extraction, and were stored at - $80^0$C until RNA extraction proceeded.

**3.2.17 RNA extraction**

Lung samples have been fully thawed at room temperature. RNA extraction was conducted by using Trizol® reagent under the manufacture's protocol. After extraction, RNA samples were purified by ethanol precipitation. Final RNA concentration was measured with a UV spectrophotometer (Nanodrop; Thermo Fisher Scientific, Inc., Massachusetts, USA).

**3.2.18 Reverse transcription**

RNA solution equivalent to 250 or 500 ng RNA was diluted with RNase-free water up to 3 or 6 µL in a PCR tube. Reverse transcription was done by using ReverTra Ace® qPCR RT Master Mix with gDNA Remover and S1000 Thermal cycler (Bio-rad Laboratories, USA), and following manufacture's protocol.

### 3.2.19 Quantitative PCR using the comparative Ct method (ΔΔCt method)

For each well, cDNA solution was diluted to 2.5 ng/µL with filtered (0.2 µm) deionized distilled water. One µL of Diluted cDNA solution was mixed with four µL of primer mixture solution (625 nM) which consisted of the following components; Thunderbird™ SYBR® qPCR Mix 2.5 µL, primers (10 µM) 0.5 µL and DDW 1.5 µL. The mixture was added into LightCycler® 480 Multiwell Plate 384; Clear (Roche Diagnostics, Basel, Switzerland). PCR was conducted with LightCycler® 480 Instrument II, 384-well (Roche Diagnostics, Basel, Switzerland) under the following conditions;

| | | |
|---|---|---|
| Pre-incubation | 1 cycle: | 95ºC, 1 minute |
| Amplification | 40 cycles: | 95ºC, 15 seconds |
| | | 55ºC, 30 seconds |
| | | 60ºC, 30 seconds |
| Melting curve | 1 cycle: | 95ºC, 5 seconds |
| | | 65ºC, 1 minute |
| | | 97ºC, cont |
| Cooling | | 40ºC, 15 seconds |

Gene expression was analyzed by the ΔΔCt method, comparing to GAPDH as a reference gene.

### 3.2.20 Preparation of GALA/MEND encapsulating gold nanoparticles (GALA/MEND-AuNPs)

Lipid solution consisted of DOTMA, Cholesterol, and EPC at the molar lipid ratio of 3/4/3. The lipid concentration was 8 mM in ethanol. In the meanwhile, 3.67 mL of AuNP solution (PELCO® NanoXactTM 5 nm 5 Cap Gold; 5 mg/mL) was mixed with 334 µL of 10 mM HEPES buffer (pH 7.4) containing 5% glucose, to prepare an aqueous solution of AuNPs.

The lipid and aqueous solutions were mixed together through a YSP-301 syringe pump (YMC, Japan) at the flow rate of 375 μL/min and 1,125 μL/min, respectively. The mixture solution was then transferred to a dialysis bag, and dialyzed in 20 mM MES buffer (pH 6.0) and subsequently PBS(-) for 1 hour each. After that, the dialysate was concentrated to 1 mL with a Himac CP702 centrifuge (Hitachi, Japan) under the following condition; 1000g, 25ºC, 12-15 minutes. Size and zeta potential were measured with a Nano-ZS Zeta Sizer (Malvern instrument, UK).

**3.2.21 *In vivo* observation with transmission electron microscopy**

GALA/MEND-AuNPs were intravenously injected via a tail vein at 2 mg AuNPs/kg. At 1 or 24 hours post-injection, mice were sacrificed by $CO_2$ asphyxiation. Lungs were flushed with HBSS(-) solution via cardiac perfusion and infused with 2.5% paraformaldehyde solution in Sorensen's phosphate buffer (pH 7.2; 0.1M) via intratracheal instillation.Then, lungs were fixated by soaking overnight in paraformaldehyde (2.5%v/v) in Sorensen's phosphate buffer (pH 7.2; 0.1M). After that, lungs were rinsed with the phosphate buffer and embedded in 2% agar block. Lung slices were prepared by cutting the blocks at the thickness of 500 μm with microslicer. The slices were processed for ultrathin sections by staining with 1% osmium tetroxide in Sorensen's phosphate buffer (pH7.2; 0.1M) and embedding with epon812 in propylene oxide. The sections were cut at the thickness of 60 nm and stained with Ti Blue solution (1:5 to 1:10 by volume; Nisshin EM, Japan). The sections were observed via a JEM-2100 electron microscope (JEOL, Japan) at the accelerating voltage of 80kV. TEM images were finally taken by a CCD camera.

### 3.3 Results

#### 3.3.1 Cytotoxicity of pharmacological inhibitors in human lung endothelial cells

The wst-8 assay was conducted in HMVEC-L to screen tolerable concentrations of endocytosis inhibitors; filipin III, chlorpromazine, and amiloride which targets caveolae pathway, clathrin pathway, and macropinocytosis, respectively.[77-80] A maximum concentration was considered as the threshold concentration by which cell viability reduced to 80%. **Figure 3-3** illustrates percentages of cell viability after treating the inhibitors at different concentrations. The viability was reduced to 80% after treating with filipin III, chlorpromazine, and amiloride at 1 µM, 5 µg/mL, and 50 µM, respectively. These concentrations were thus selected as the highest concentrations for applying in the inhibitory assay.

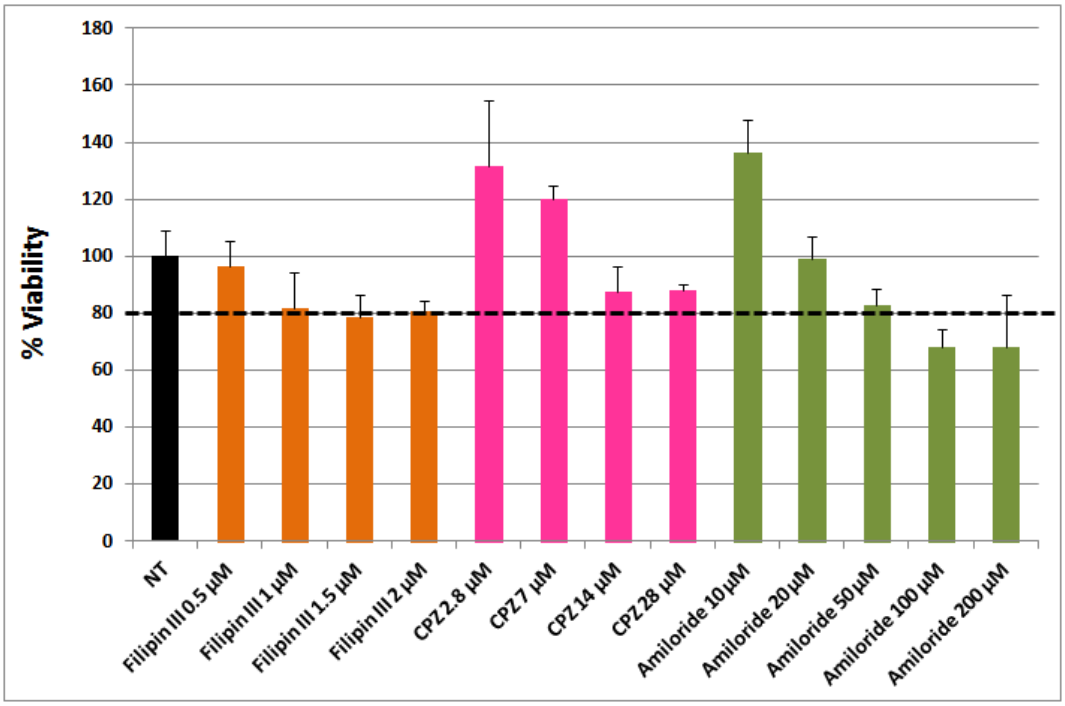


**Figure 3-3** Cell viability of HMVEC-L after treating the pharmacological inhibitors at different concentrations. Data were represented as mean ± SD; n= 3-6.

#### 3.3.2 Endocytosis inhibition against GALA/Chol-LPs in human lung endothelial cells

After screening optimal concentrations of the inhibitors, the uptake inhibition of GALA/Chol-LPs was evaluated in HMVEC-L at 3 hours. As a result, the cellular uptake was significantly decreased by chlorpromazine in a dose-dependent manner, by 28% and 52% at

the concentration of 2.5 and 5 μg/mL, respectively **(Figure 3-4)**. Such inhibition was not observed after applying either filipin III or amiloride. As a consequence, clathrin-mediated endocytosis was assumed to be the main uptake mechanism for GALA/Chol-LPs into lung endothelium.

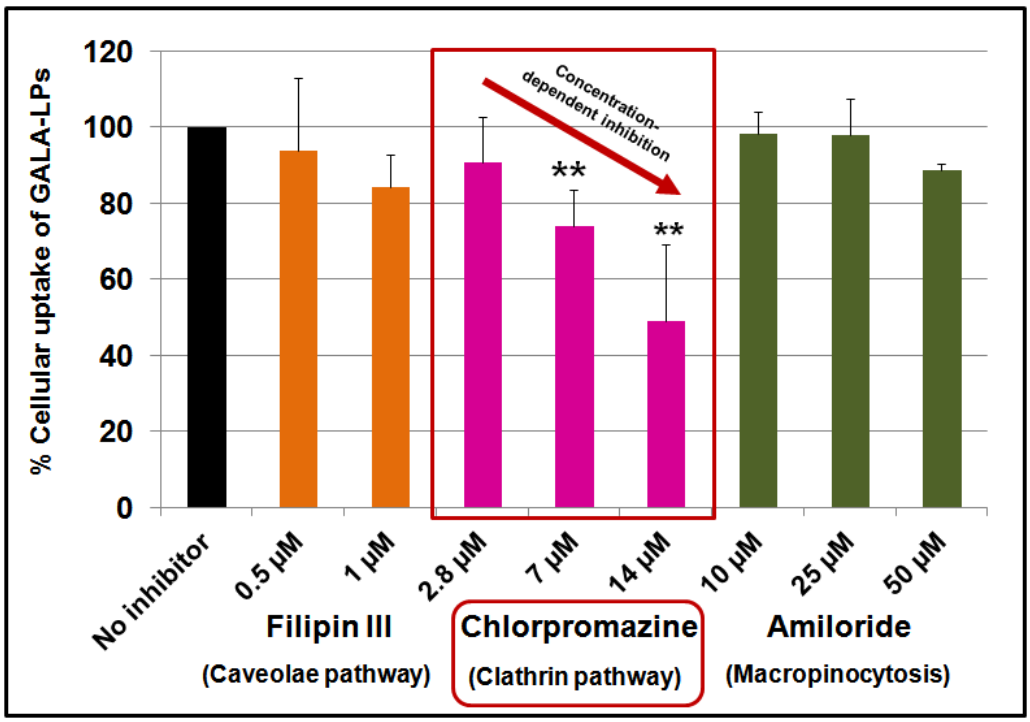


**Figure 3-4** Cellular uptake of GALA/Chol-LPs after treating the inhibitors at various concentrations. Data were represented as mean±SD. (n=3-4) *p<0.05 vs. NT; One-way ANOVA followed by Bonferroni's test.

### 3.3.3 Cellular internalization of co-incubated GALA/Chol-LPs and endocytosis markers

As reported above, clathrin pathway was identified as an uptake route for GALA/Chol-LPs into lung endothelial cells. To confirm this notion, cellular internalization of GALA/Chol-LPs was visualized via confocal microscopy in HMVEC-L. DiI-labeled GALA/Chol-LPs were co-incubated with different kinds of endocytosis markers; CTB, transferrin, and dextran for caveolae pathway, clathrin pathway, and macropinocytosis, respectively.[79,81-84] The uptake pathway was distinguished by colocalization between GALA/Chol-LPs and each marker at 2 hours after treating the liposomes. The observation revealed that GALA/Chol-LPs were vividly co-localized with transferrin in HMVEC-L **(Figure 3-5b)**. In contrast, the colocalization was hardly observed after treating either CTB **(Figure 3-5a)** or dextran **(Figure 3-5c)**. This finding is in good agreement with the results

from endocytosis inhibition. Therefore, clathrin was proved to have an essential role to facilitate an internalization of GALA-modified nanocarriers.

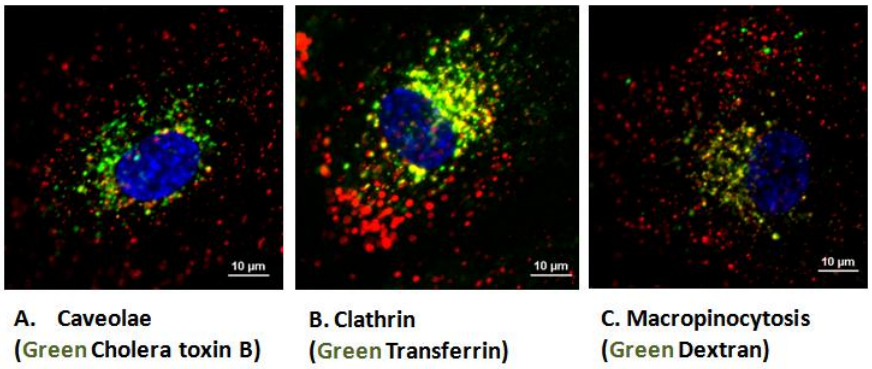


**Figure 3-5** Confocal images represents the colocalization between GALA/Chol-LPs and endocytosis markers; (A) CTB for caveolae pathway, (B) Transferrin for clathrin pathway, and (C) Dextran for macropinocytosis pathway. Red: liposomes (DiI), Green: endocytosis markers. Scale: 10 µm.

### 3.3.4 Synthesis of GALA/PEG$_{5000}$

GALA/PEG$_{5000}$ was prepared by conjugating cysteine-terminated GALA **(Cys-GALA; Figure 3-6A)** with DSPE-PEG$_{5000}$-MAL **(Figure 3-6B)** via Micheal reaction in ethanol (**Figure 3-7)**.[64] The conjugation was then confirmed by MALDI-TOF MS. The mass peak (m/z) was shifted 5452.216 of DSPE-PEG$_{5000}$-MAL **(Figure 3-6B)** to 9018.106 after GALA conjugation **(Figure 3-8)**. Since the change in the average molecular weight is comparable to that of Cys-GALA, that confirms that the GALA/PEG$_{5000}$ was successfully synthesized.

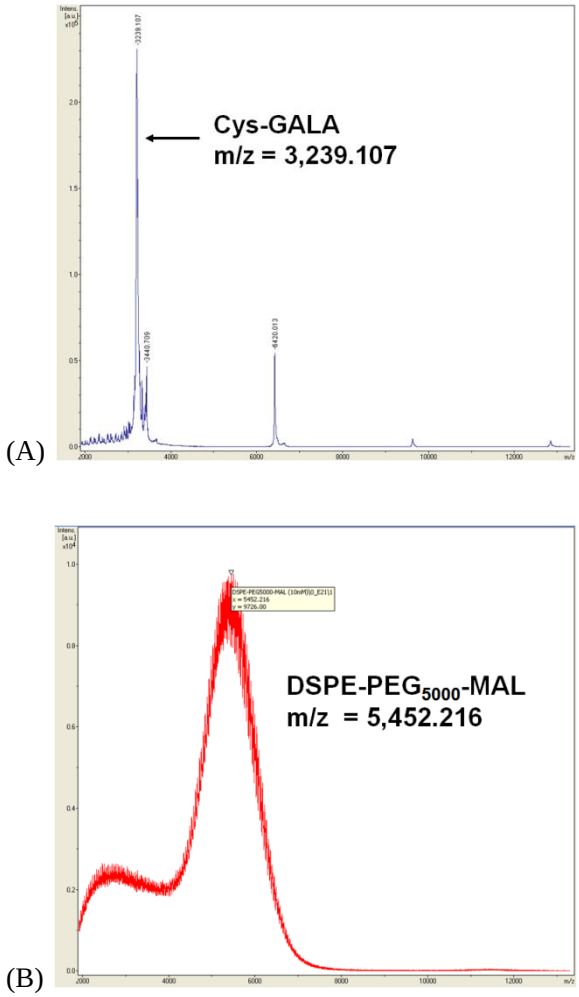


**Figure 3-6** MALDI-TOF MS spectra of (a) Cys-GALA and (b) DSPE-$PEG_{5000}$-MAL

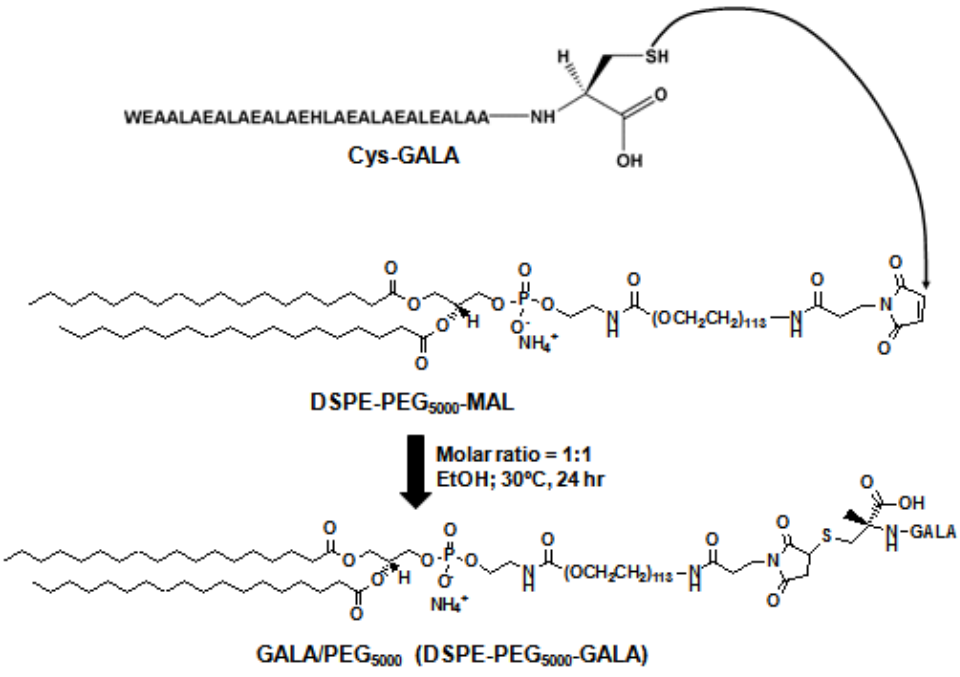


**Figure 3-7** A schematic illustration represents synthesis of GALA/$PEG_{5000}$

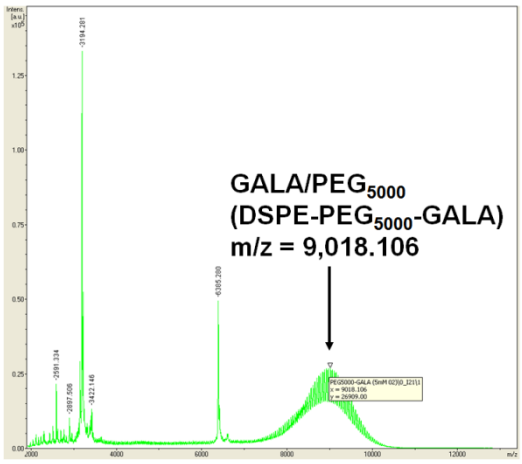


**Figure 3-8** MALDI-TOF MS spectra of GALA/$PEG_{5000}$

### 3.3.5 Gating population of lung endothelium and type I alveolar epithelium by flow cytometry

Lung endothelium (EC) and type I alveolar epithelium (ATI) [85] were stained with different combinations and were sorted by flow cytometry. The EC population was enriched by double staining with PE-conjugated anti-mouse CD31 antibody and FITC-conjugated anti-mouse CD45 antibody. The endothelial marker, CD31 is strongly expressed in alveolar capillaries of the lung.[86] However, CD31 is also expressed in various kinds of myeloid cells such as monocytes, neutrophils, and dendritic cells.[87,88] The anti-CD45 antibody was then applied to exclude immune cells from EC.[89] By double staining, the gated EC **(Figure 3-9A)** was occupied approximately by 20-30% from a total gated population. The absence of gated population was observed when cells were stained with isotype controls **(Figure 3-9B)**, thus the staining condition was suitable for EC.

The ATI population was classified by multiple staining of anti-CD31, anti-CD45, anti-EpCAM and anti-Podoplanin antibodies. As podoplanin has been reported as the ATI-selective marker[90-92], the PE anti-hamster podoplanin

antibody was combined with the PE-Cy7 EpCAM antibody to identify the ATI. FITC-conjugated anti-CD31 and anti-CD45 antibodies were also included to exclude both EC and myeloid cells from the gated population. The gated ATI **(Figure 3-10)** has the proportion of 4-10% from a total gated population. The ratio of the gated EC and ATI was in proximity with the amount which was reported elsewhere.[93,94] The absence of gated population was observed after staining cells with isotype controls. Therefore, the staining condition was suitable for ATI.

(A)

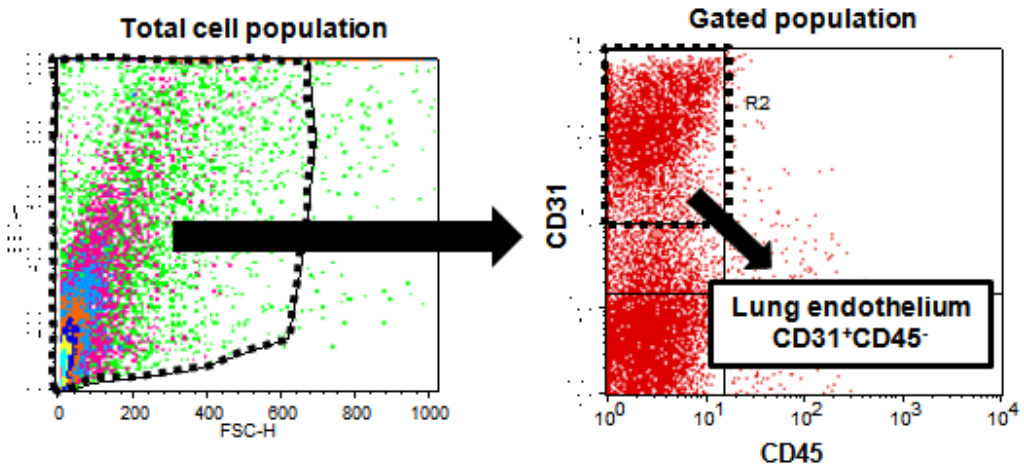


(B)

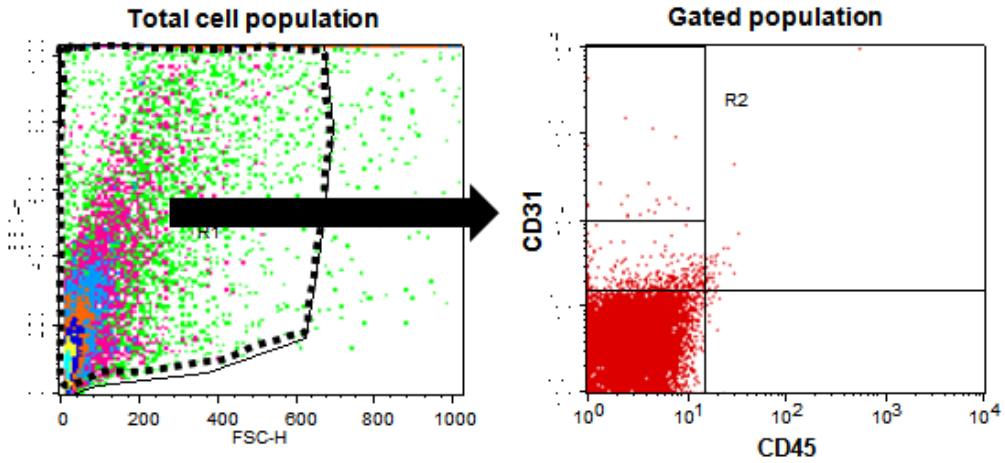


**Figure 3-9** A dot plot represents a gating population of lung endothelium after staining pulmonary cells with (A) FITC-conjugated anti-CD45 mAb and PE-conjugated anti-CD31 mAb or (B) Isotype control antibodies

(A)

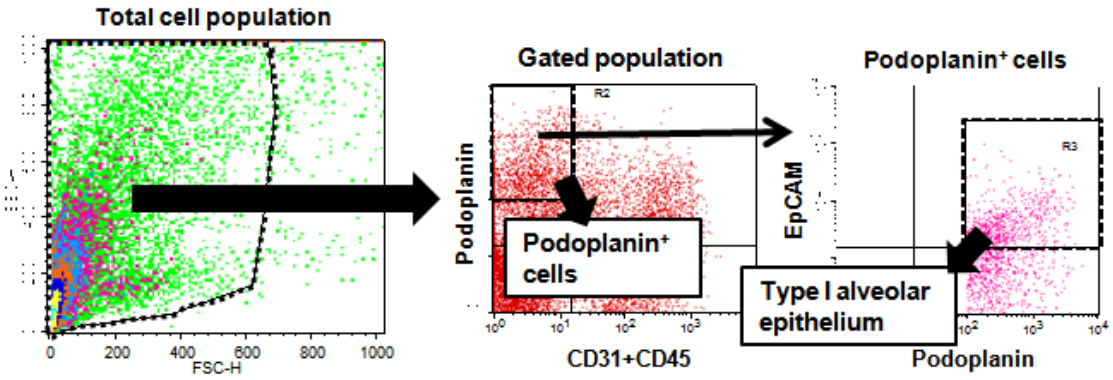


(B)

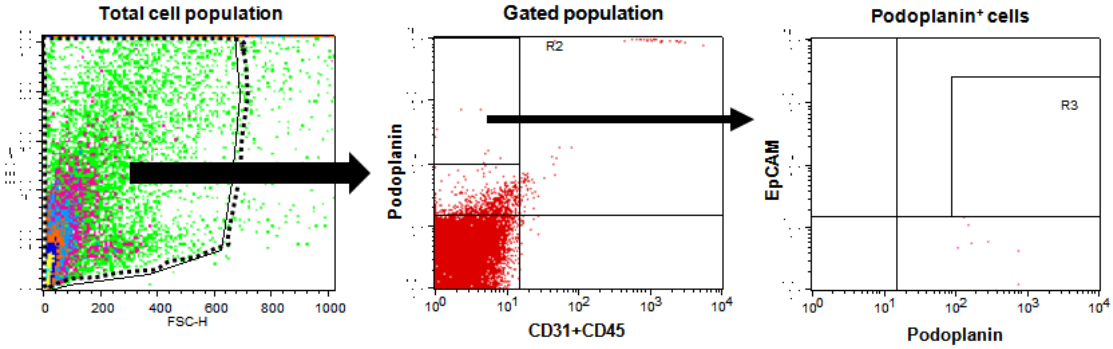


**Figure 3-10** A dot plot represents a gating population of type I alveolar epithelium after staining pulmonary cells (A) with FITC-conjugated anti-CD45 mAb, FITC-conjugated anti-CD31 mAb, PE-conjugated anti-podoplanin mAb and PE-Cy7 conjugated anti-EpCAM (CD326) mAb or (B) Isotype control antibodies

### 3.3.6 Accumulation of GALA-LPs in lung endothelium

Liposome accumulation in EC which was identified in section 4.3.1 was quantitated by flow cytometry. As shown in **Figure 3-11A**, a histogram of DiD fluorescence represented as bell-shaped curves. Each curve in blue, light blue and green represented the accumulation of GALA/Chol-LPs, GALA/$PEG_{2000}$-LPs, and GALA/$PEG_{5000}$-LPs, respectively. In the meanwhile, PEG-LPs which were illustrated as a steep red curve were little detected for the accumulation.

DiD(+) cells were defined as the cells which internalized GALA-LPs in EC. These cells were counted from the histogram curve **(Figure 3-11B)**. PEG-LPs were hardly taken up in EC since negligible percentages of DiD(+) cells were detected. Meanwhile, more than 70% of total ECs showed the uptake of GALA-LPs. The degree of liposome accumulation was further evaluated by measuring DiD fluorescent intensity in DiD(+) cells **(Figure 3-11C)**. The significant uptake was confirmed for all kinds of GALA-LPs. Compared to direct conjugation of GALA to cholesterol (GALA/Chol), conjugating GALA to PEG linkers (GALA/$PEG_{2000}$ and GALA/$PEG_{5000}$) led to an increasing trend of liposome accumulation in EC. The accumulation of GALA-LPs reached the maximum for GALA/$PEG_{5000}$-LPs. These results stressed targeting activity of GALA to EC. An enhancing effect of PEGylation on targeting activity of GALA was also supported.

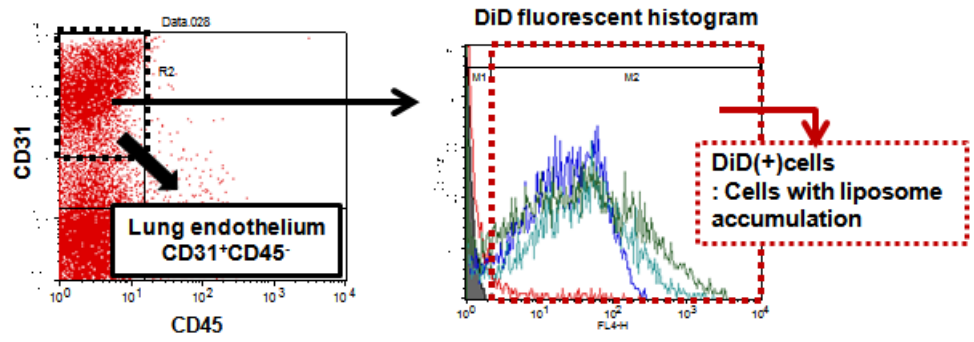


(A)

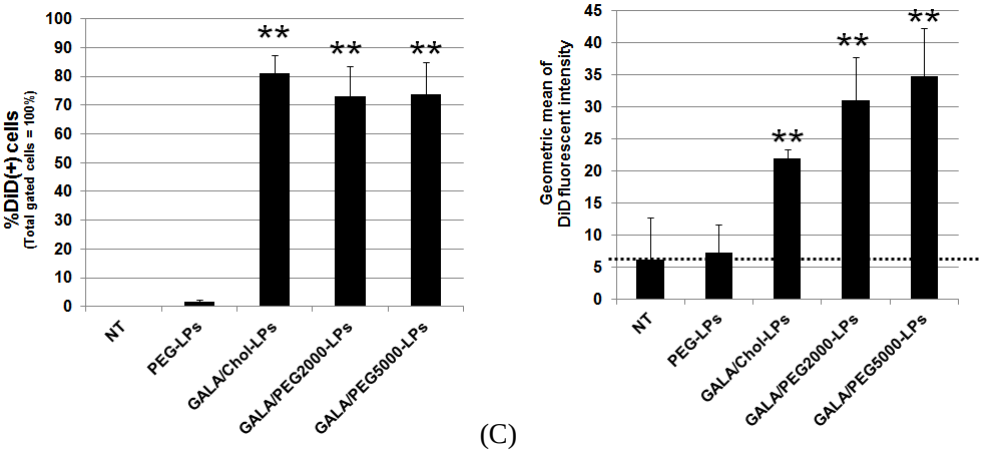


(B) (C)

**Figure 3-11** (A) A fluorescent histogram represents the extent of liposome accumulation in lung endothelium. DiD(+) cells were defined as the lung endothelial cells which showed liposome accumulation. Filled gray: non-treated, Red: PEG-LPs, Blue: GALA/Chol-LPs, Light Blue: GALA/$PEG_{2000}$-LPs, Green: GALA/$PEG_{5000}$-LPs (B) A bar graph indicates the percentage of DiD(+) cells from whole lung endothelial cells. (C) A bar graph indicated the geometric mean of DiD fluorescence intensity from DiD(+) cells in lung endothelium. Data were represented as mean ± SD; n=3. ***p*<0.01 vs. PEG-LPs; one-way ANOVA followed by Bonferroni's test.

### 3.3.7 Accumulation of GALA-LPs in type I alveolar epithelium

In addition to EC, liposome accumulation in ATI which was identified in section 4.3.1 was measured by flow cytometry. As shown in **Figure 3-12A**, a histogram of DiD fluorescence represented as bell-shaped curves. Each curve in blue, light blue and green represented the accumulation of GALA/Chol-LPs, GALA/$PEG_{2000}$-LPs, and GALA/$PEG_{5000}$-LPs, respectively. In the meanwhile, PEG-LPs which were illustrated as a steep red curve were little detected for the accumulation.

DiD(+) cells were defined as the cells which internalized GALA-LPs in ATIs. These cells were counted from the histogram curve **(Figure 3-12B)**. More than 30% of total ATIs were detected for the uptake of GALA-LPs. The degree of liposome accumulation was further evaluated by measuring DiD fluorescent intensity in DiD(+) cells **(Figure 3-12C)**. GALA-LPs were confirmed for a significant uptake in ATI. Among all GALA-LPs, GALA/$PEG_{2000}$-LPs had the highest accumulation in ATI. These results highlighted the role of GALA to promote transendothelial activity.

(A)

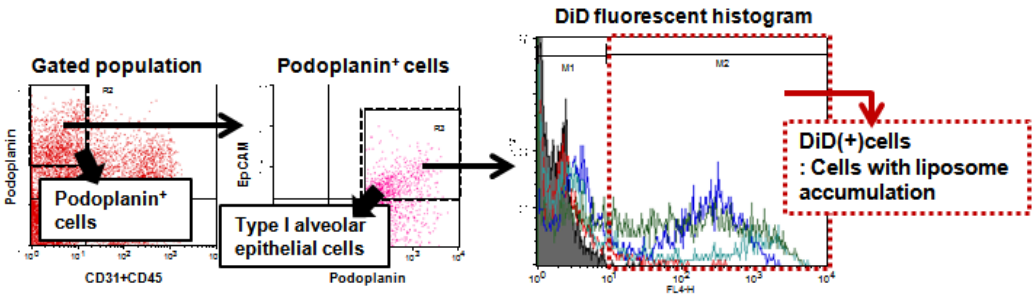


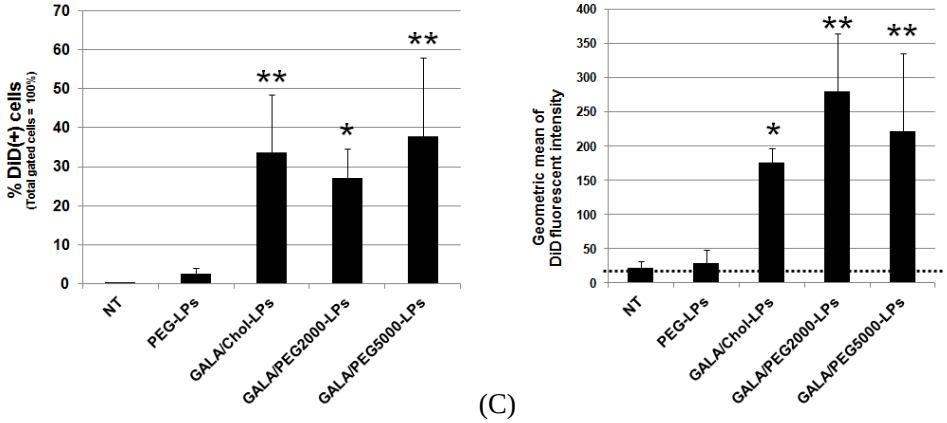


(B) (C)

**Figure 3-12** (A) A fluorescent histogram represents the extent of liposome accumulation in Type I alveolar epithelium. DiD(+) cells were defined as the type I alveolar epithelial cells which showed liposome accumulation. Filled gray: non-treated, Red: PEG-LPs, Blue: GALA/Chol-LPs, Light Blue: GALA/$PEG_{2000}$-LPs, Green: GALA/$PEG_{5000}$-LPs (B) A bar graph indicates the percentage of DiD(+) cells from whole type I alveolar epithelial cells. (C) A bar graph indicated the geometric mean of DiD fluorescence intensity from DiD(+) cells in Type I alveolar epithelium. Data were represented as mean ± SD; n=3. *$p$<0.05, **$p$<0.01 vs. PEG-LPs; one-way ANOVA followed by Bonferroni's test.

### 3.3.8 Silencing activity of GALA-MEND in type I alveolar epithelium

Transcytosis activity was further evaluated by silencing effect of GALA/MEND in ATIs. The ATI-specific marker, podoplanin (Pdpn) was chosen as the silencing targeting. At 1.5 siRNA mg/kg, GALA/Chol-MEND and GALA/$PEG_{2000}$-MEND significantly reduced pdpn mRNA expression by 29% and 24%, respectively **(Figure 3-13)**. In contrast, GALA-$PEG_{5000}$/MEND did not show the similar activity even though the accumulation in the alveolar epithelium was confirmed for in section 4.3.3.

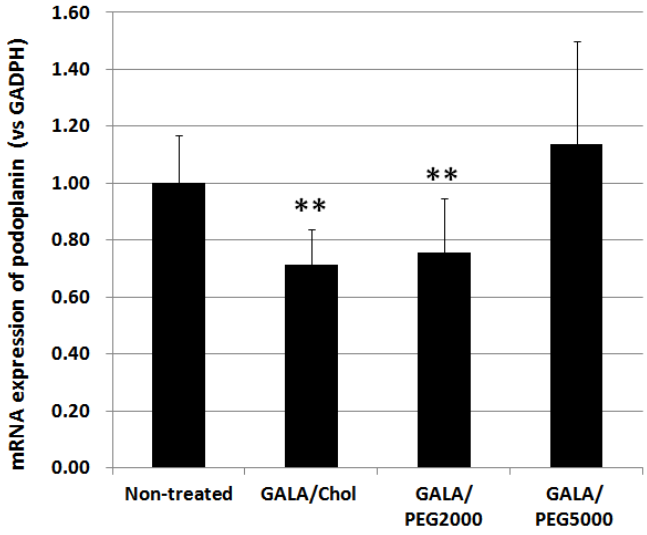


**Figure 3-13** *In vivo* pdpn knockdown activity by GALA/MEND with different GALA linkers (GALA/Chol, GALA/$PEG_{2000,}$ and GALA/$PEG_{5000}$). Data were represented as mean±SD. (n = 8-11) *$p < 0.05$ vs. NT; One-way ANOVA followed by Bonferroni's test.

### 3.3.9 Localization of GALA-MEND encapsulating gold nanoparticles (GALA/MEND-AuNPs) in lung tissues

Transcytosis activity of GALA was evaluated by transmission electron microscopy (TEM). In the non-treated lung, an air-blood barrier was shown as a separate layer of EC, a basement membrane and ATI from inside to outside **(Figure 3-14)**. To visualize the transendothelial activity of GALA by TEM, AuNPs were then encapsulated in GALA/MEND by microfluidic mixing. GALA/MEND-AuNPs could be formed with an average diameter less than 80 nm with homogenous size distribution **(Table 3-3)**

(A)

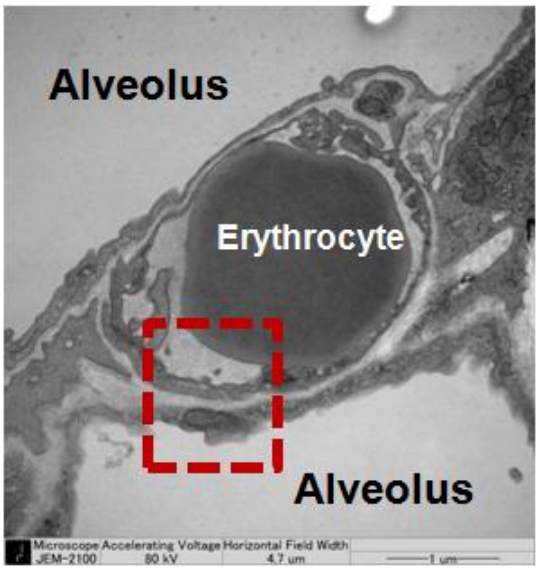


(B)

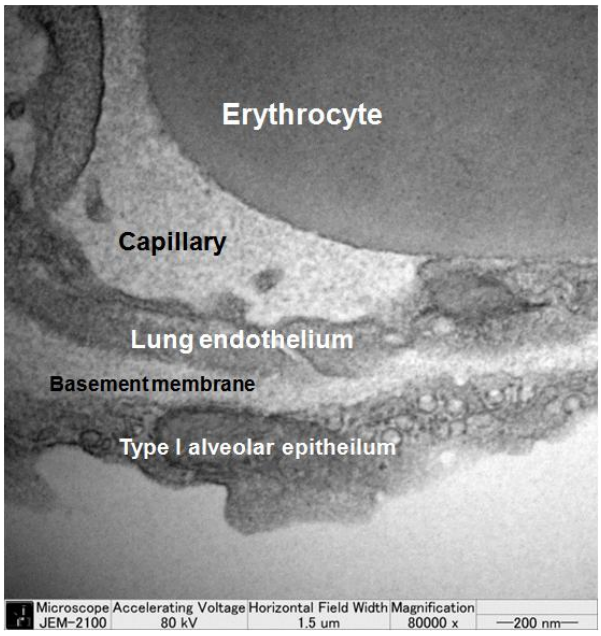


**Figure 3-14** TEM images of an air-blood barrier inside the non-treated lung at the magnification of (A) x20,000 and (B) x80,000. The image (B) shows the magnified area from the red box in (A).

**Table 3-3** Physical properties of GALA/MEND encapsulating gold nanoparticles (GALA/MEND-AuNPs) (n=1)

| | Diameter (nm) | PDI | Zeta potential (mV) |
|---|---|---|---|
| GALA/MEND-AuNPs | 73.17 nm | 0.190 | +10.7 mV |

Ultrathin sections of lung tissues were observed at 1-hour post-administration. As shown in **Figure 3-15B**, AuNPs were observed as black spots inside the air-blood barrier. Most AuNPs were internalized into EC (Black circles in **Figure 3-15B**). More interestingly, AuNPs were also located inside the basement membrane (Red circles in **Figure 3-15B**) and reached AT (Yellow circles in **Figure 3-15B**). These findings highlighted that GALA/MEND could penetrate EC and transport AuNPs to other layers in the membrane.

Furthermore, GALA/MENDs were found the ability to deliver AuNPs to other tissues in the lung. As shown in **Figure 3-16B**, AuNPs were taken up in type II alveolar epithelium (ATII). Some particles were localized in the cytosol (Black circles in **Figure 3-16B**) and at the edge of lamellar bodies (Yellow circles in **Figure 3-16B**). Not only in ATII, but AuNPs were also trapped inside an alveolar macrophage as single particles (Black circles in **Figure 3-17B**) or clusters (Yellow circles in **Figure 3-17B**). These images revealed the ability of GALA/MEND to transport AuNPs to all tissues beyond EC.

(A)

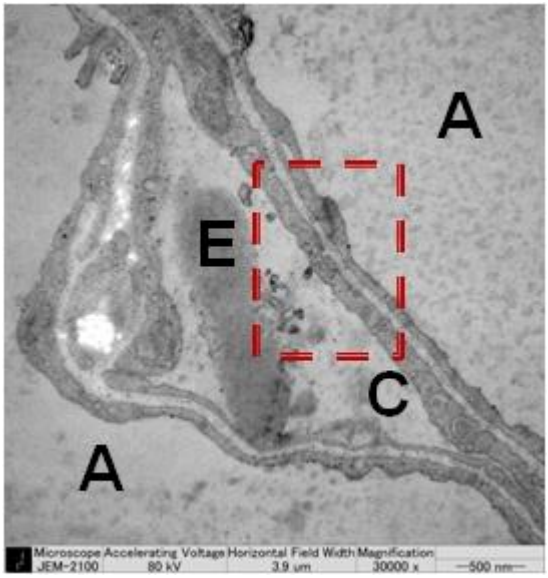


(B)

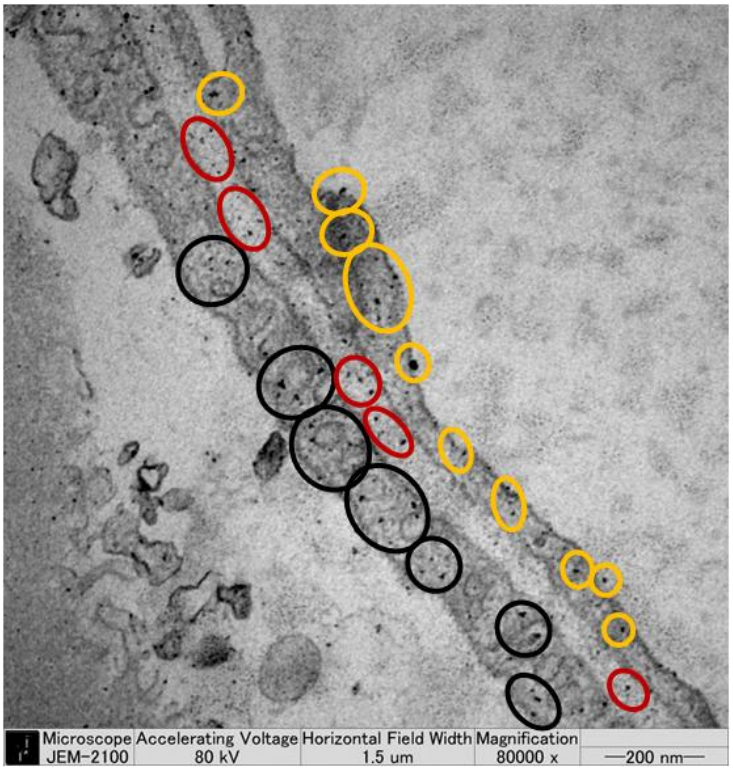


**Figure 3-15** TEM images of an air-blood barrier inside the lung treated with GALA/MEND-AuNPs at the magnification of (A) x30,000 and (B) x80,000. The image (B) shows the magnified area from the red box in (A). Black, red and yellow circles represent AuNPs inside lung endothelium, basement membrane and type I alveolar epithelium, respectively. These images were taken at 1-hour post-administration.

(A)

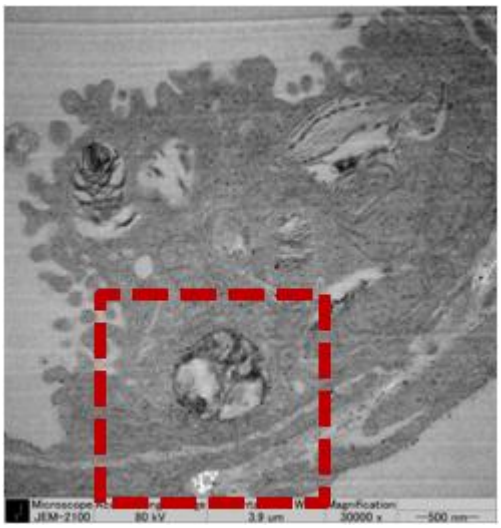


(B)

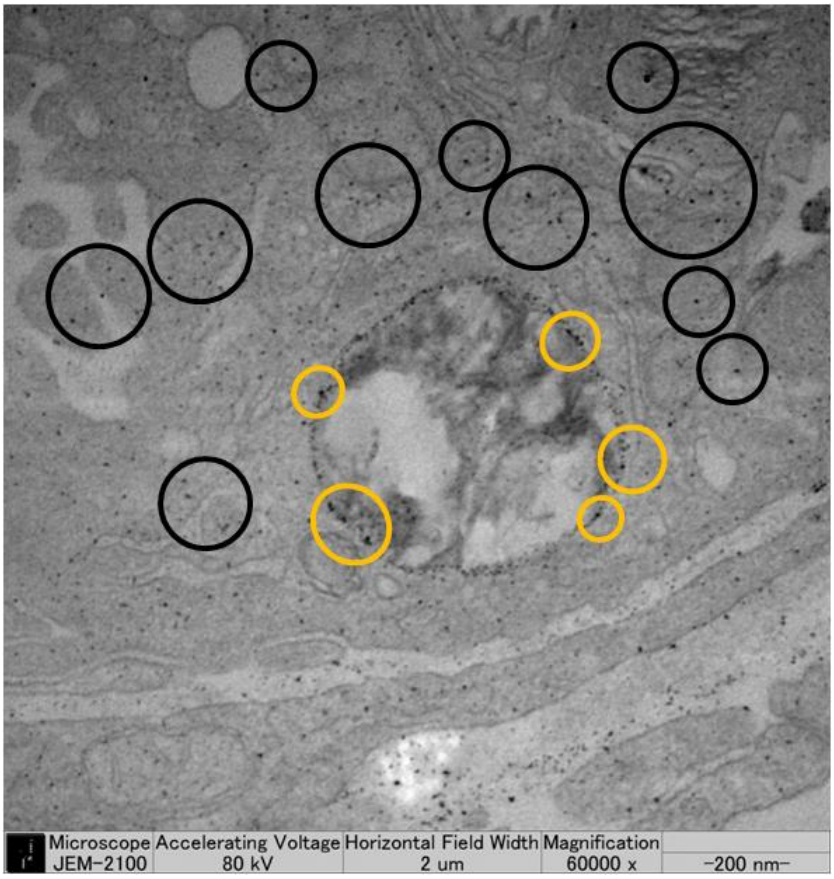


**Figure 3-16** TEM images of type II alveolar epithelium inside the lung treated with GALA/MEND-AuNPs at the magnification of (A) x30,000 and (B) x60,000. The image (B) shows the magnified area from the red box in (A). Black and yellow circles represent AuNPs inside the cytosol and around lamellar bodies, respectively. These images were taken at 1-hour post-administration.

(A)

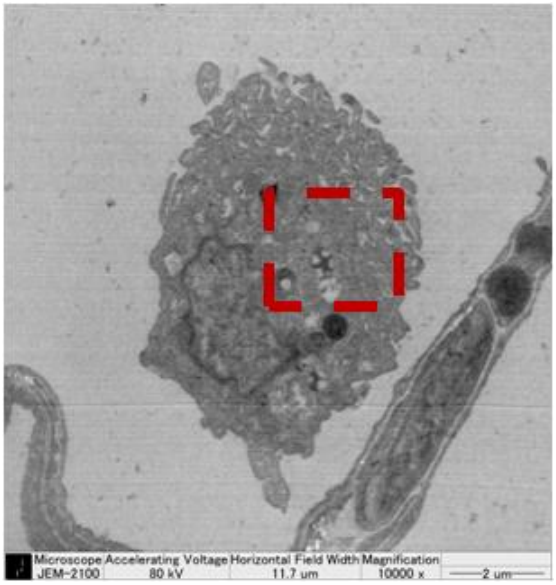


(B)

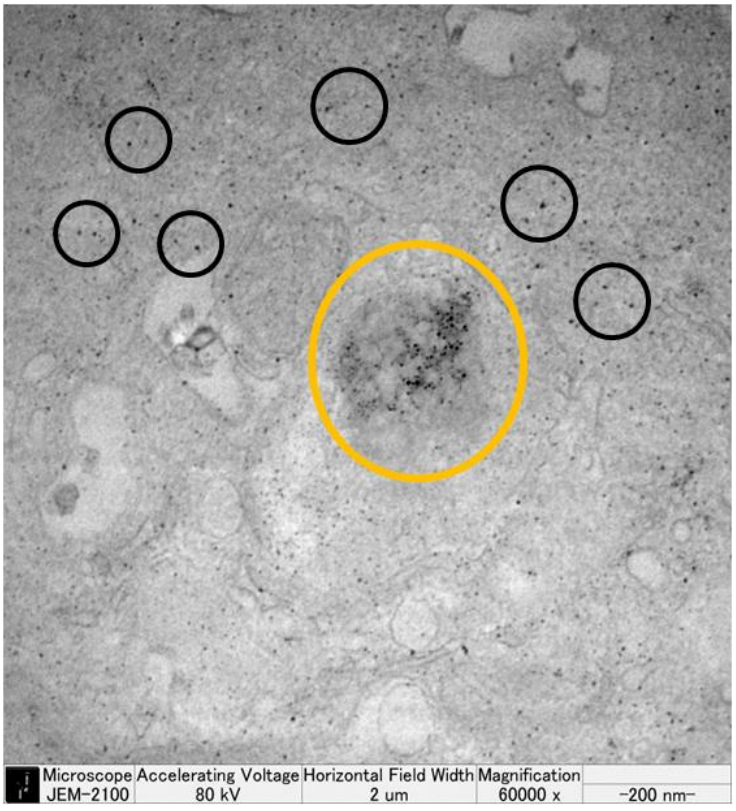


**Figure 3-17** TEM images of an alveolar macrophage inside the lung treated with GALA/MEND-AuNPs at the magnification of (A) x30,000 and (B) x60,000. The image (B) shows the magnified area from the red box in (A). Black and yellow circles represent single AuNPs and clusters of AuNPs, respectively. These images were taken at 1-hour post-administration.

\

**3.4 Discussion**

GALA has been investigated for a binding mechanism on lung endothelial surfaces.[19] However, detailed studies regarding cellular trafficking are still lacking. In this part, an uptake pathway and a transendothelial activity of GALA-modified nanocarriers were examined.

Several publications have documents that caveolae-mediated pathway is an active transport pathway in endothelial cells since caveolae occupy by 95% of cell surface vesicles and 20% of cell volume.[95] Nevertheless, filipin III which is an inhibitor of the caveolae pathway did not reduce the cellular internalization of GALA/Chol-LPs **(Figure 3-4)**. Besides, the liposomes were not co-localized with cholera toxin B which is a marker for this pathway **(Figure 3-5A)**. As a consequence, caveolae-mediated endocytosis does not represent the uptake route for GALA/Chol-modified nanocarriers.

Previous studies indicate that influenza virus, which is the design model of GALA, is mainly taken up by the clathrin-mediated endocytosis.[72,96,97] Furthermore, the virus was internalized into the cells via a dynamin-independent pathway under the inhibition of clathrin pathway.[98] The detailed investigation revealed that macropinocytosis is an alternative entry route for influenza virus.[99] In contrast, macropinocytosis was proved not to be the entry mechanism for GALA/Chol-LPs, because amiloride could not suppress internalization **(Figure 3-4)**. Furthermore, co-localization was undetected between the liposomes and dextran **(Figure 3-5C)**. Instead, the liposome uptake was profoundly inhibited after pre-treating lung endothelial cells with chlorpromazine which disrupts the clathrin-mediated pathway **(Figure 3-4)**. In addition, the co-localization was remarkable between the liposomes and a clathrin marker, transferrin **(Figure 3-5B)**. As a consequence, unlike influenza virus, the clathrin-mediated pathway was assumed as an internalization route for GALA-LPs in lung endothelial cells **(Figure 3-18)**.

In addition to the caveolae pathway, previous publications demonstrated the clathrin pathway as an endocytosis route in rat lung endothelial cells. Expression of clathrin heavy chain was detected in rat lung endothelial cells by confocal microscopy and immunoblotting.[100] Furthermore, the uptake of antitrypsin was strongly inhibited by

chlorpromazine in lung endothelium.[95] Taken together, the clathrin-mediated endocytosis could be recognized as an alternative uptake route in lung endothelial cells.

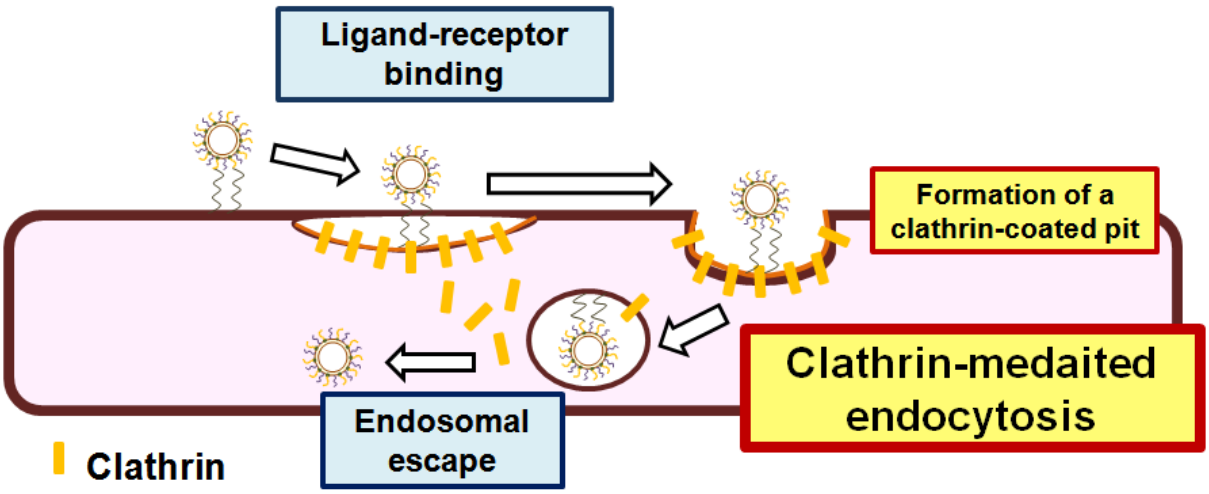


**Figure 3-18** A graphical illustration demonstrates the uptake of GALA-modified nanocarriers via clathrin-mediated pathway

GALA-LPs were found to extravasated blood vessels as shown in **Figure 3-1**. Thus, it was assumed that GALA could function endothelial transcytosis in a lung. GALA-modified nanoparticles were hypothesized to move across EC and reach ATI **(Figure 3-2)**. In this part, transcytosis activity was also examined to prove this hypothesis.

In general, transwell systems have been used as ideal *in vitro* models to evaluate transcytosis of macromolecules and nanoparticles in an endothelial monolayer[101-103] or an endothelial-epithelial bilayer[104,105]. Transcytosis activity would be determined by concentration or an amount of tested compound, which penetrated the apical side to the basolateral (bottom) side of a cell monolayer in an insert and/or the lower supernatant in a Transwell chamber. However, this assay suffers from series of limitations which hinder an accurate quantification.[106] For example, fluorescent labeling with a labile dye retains in the chamber due to insufficient cleaning, leading to false positive signals . In the meanwhile, dye release due to degradation of nanoparticles could be misinterpreted as transendothelial transport. Nanoparticle agglomeration either in the culture media or after internalization is likely to impair the assay because agglomerates obstruct filter pores inside an insert. In addition, treating endothelial cells with pharmacological compounds was reported for disrupting monolayer integrity due to widened paracellular gaps.[107]

In an effort to evaluate transendothelial activity in the actual physiological barrier, *in vivo* measurements were developed. Flow cytometry was first performed to measure the accumulation of GALA-LPs in ECs and ATIs. As anticipated, GALA-LPs were shown for the accumulation in the majority of ECs **(Figure 3-11)**. These results correlate fairly well with the *in vitro* studies previously reported.[19] The quantitative extent of liposome uptake is also consistent with confocal images from the third part, as GALA/$PEG_{2000}$- and GALA/$PEG_{5000}$-LPs had a higher uptake than GALA/Chol-LPs. Furthermore, GALA/$PEG_{5000}$-LPs were accumulated in ECs more than GALA/$PEG_{2000}$-LPs. Our results regarding PEG linker length share a number similarities with the findings reported by Shiokawa et al.[61] and Yamada et al.[62]. Longer PEG linkers were reported to enhance ligand association with cell surface receptors, by increasing binding frequencies and lengthening adhesion time of ligands and receptors.[61,108,109] Therefore, conjugating GALA with $PEG_{5000}$ seems likely to promote binding interactions between liposomes and sugar receptors on lung endothelial cells.

More surprising results were demonstrated when the accumulation of GALA-LPs was also observed in ATIs. Compared to ECs (> 70% of total ECs), relatively small fractions of ATIs (30% of total ATIs) showed the uptake of GALA-LPs **(Figure 3-12)**. However, mean fluorescence intensity from GALA-LPs was relatively higher in ATIs **(Figure 3-12C)** than in ECs **(Figure 3-11C)**. These differences are likely to indicate distinct patterns of liposome internalization in both cells. GALA-LPs might be distributed thoroughly in most ECs, whereas they are supposed to concentrate on the tiny amount of ATIs. The possible explanation behind this assumption is that an extracellular matrix (ECM) lining between ECs and ATI might impede translocation of the liposomes to ATIs. ECM consists of a basement membrane which a thin layer of type IV collagen is sandwiched in the middle of an extracellular matrix, to strengthen an air-blood barrier.[110] The basement membrane is fused with ECs and ATIs to form a thin side (approximately 0.2 – 0.3 μm) for gas exchange. In contrast, the thicker side (up to 1 μm) includes type I collagen fibers to support lung structure, as well as interstitial cells, such as fibroblasts and pericytes to regulate fluid exchange across the pulmonary capillary.[110] As a consequence, variations in the barrier thickness are possible to restrict the particle movement after departing ECs, so that the uptake would be

limited in ATIs. The influence of ECM on transendothelial activity is substantiated by partial silencing activity against an ATI marker, podoplanin by GALA/Chol-MEND and GALA/$PEG_{2000}$-MEND **(Figure 3-13)**.

Transcytosis of GALA/MEND-AuNPs was further observed by TEM. This method represents a useful alternative to visualize nanoparticles in the lung at nanoscale levels.[111,112] The most striking result to emerge from TEM observation is that AuNPs were translocated beyond ECs. The particles resided in the basement membrane as well as in ATI (Red and yellow circles in **Figure 3-15B**). AuNPs resided not only inside an air-blood barrier, but also in ATII **(Figure 3-16B)** and an alveolar macrophage **(Figure 3-17B)**.

In general, lung endothelium is classified as continuous endothelium which restricts paracellular transport of solute with a molecular diameter of up to 6 nm.[113] It has been proposed by Li et al.[114] that AuNPs increased endothelial paracellular permeability by compromising the integrity of tight junctions. Evans blue dye leaked from a brain-blood barrier at 24 hours after intravenous injection of AuNPs. There was thus a concern about enhanced paracellular transport in the transcytosis study. However, the administration dose of GALA/MEND-AuNPs was relatively low, and the lung was observed merely at 1 hour. A negative effect on endothelial structures was not supposed to occur. Besides, since GALA/MEND-AuNPs were prepared at a high lipid concentration, encapsulation efficiency of AuNPs was expected to be 100%. Presumably, AuNPs encapsulated in GALA/MEND might enter into lung endothelium via a transcellular pathway rather than a paracellular pathway.

One question still unanswered is which kind of mechanism regulates transcytosis activity of GALA. Caveolae are the critical effector to control endothelial transcytosis in the lung.[102,112] They are 60-80 nm wide pit in the plasma membrane, representing 50–70% of the lung EC surface membrane and occupying 10–15% of the total cell volume.[115,116] Caveolae were confirmed for a role in the transendothelial transport of protein and antibody by using TEM.[112,117] Unfortunately, caveolae could not be detected in TEM images of GALA/MEND-AuNPs.

On the contrary, since GALA-modified nanocarriers are taken up into endothelial cells via a clathrin-mediated pathway, clathrin would possibly regulate lung transcytosis of the nanocarriers. A role of clathrin in endothelial transcytosis was reported in several publications. In microvascular endothelial cells, Insulin transcytosis was significantly reduced by chlorpromazine and clathrin silencing.[118] In addition, clathrin inhibition by chlorpromazine and potassium depletion also disturbed a transendothelial transport of antibody across a blood-brain barrier.[119] Further investigation is required to examine clathrin function in lung transcytosis of GALA.

### 3.5 Conclusion

This study has clarified cellular trafficking of GALA-modified nanocarriers in the lung. First, a clathrin-mediated pathway was an uptake route for GALA-modified nanocarriers in lung endothelium. Second, GALA functions transcytosis activity in a lung. GALA-modified nanocarriers were demonstrated for penetrating lung endothelium and being translocated into other lung tissues, such as type I and II alveolar epithelium and alveolar macrophages. I am confident that these findings may improve knowledge about the cellular trafficking of GALA. Further work will concentrate on the application of transendothelial activity to develop potent lung-targeting nanocarriers by GALA.

# Summary

In this Ph.D. dissertation, GALA was investigated for enhancing lung-targeting function and elucidating further cellular mechanisms. The targeting activity of GALA was successfully improved by the following approaches:

1. The combination between GALA and a pH-sensitive lipid, YSK: This strategy could improve the intracellular activity of GALA-modified nanocarriers, because both GALA and YSK constitutively increased endosomal fusion activity. More YSK lipids have been synthesized in order to potentiate membrane fusion. These lipids will be further investigated to find the optimal lipid composition which promotes lung-targeting GALA function.

2. PEGylation of GALA: Conjugation of PEG linkers to GALA could increase lung accumulation of GALA-modified nanocarriers. PEG conjugates of GALA will be applied to design the nanocarriers which are more internalized into the lung.

Moreover, cellular mechanisms of GALA have been clarified in this project.

1. GALA-modified nanocarriers are taken up into lung endothelial cells by the clathrin-mediated pathway. The uptake mechanism is similar to the entry of influenza virus which is the design model for GALA. This study has provided more insights regarding intracellular trafficking of GALA.

2. GALA possesses an additional function as a transcytosis-targeting ligand in lung endothelium. GALA-modified nanocarriers penetrate lung endothelium to other parts of lung tissues, such as alveolar epithelium and macrophages.

These findings will open more directions to utilize GALA for developing potent lung-targeting nanocarriers.

# References


1. WHO (2017) The top 10 causes of death. Fact Sheets: World Health Organization.

2. 岩﨑容子, 渡三佳 (2015) 平成 26 年(2014)患者調査の概況. 厚生労働省.

3. 岩﨑容子, 本木久美子 (2015) 平成 26 年度国民医療費の概況. 厚生労働省.

4. Van de Graff KM, Strete D, Creek CH (2001) Respiratory System. Van De Graaff: Human Anatomy. 6th ed. New York, USA: McGraw-Hill. pp. 602-633.

5. Aird WC (2007) Phenotypic heterogeneity of the endothelium: II. Representative vascular beds. Circ Res 100: 174-190.

6. Barrett KE, Boitano S, Barman SM, Brooks HL (2010) Pulmonary function. Ganong's Review of Medical Physiology. 23rd ed. New York, USA: McGraw-Hill. pp. 587-607.

7. Lung anatomy and structure infographic. LifeMap Discovery: Lifemap Sciences, Inc.

8. Muzykantov VR (2013) Targeted Drug Delivery to Endothelial Adhesion Molecules. ISRN Vascular Medicine 2013: 27.

9. Fuhr U (2000) Induction of Drug Metabolising Enzymes. Clinical Pharmacokinetics 38: 493-504.

10. Takakura Y, Hashida M (1996) Macromolecular Carrier Systems for Targeted Drug Delivery: Pharmacokinetic Considerations on Biodistribution. Pharmaceutical Research 13: 820-831.

11. Grislain L, Couvreur P, Lenaerts V, Roland M, Deprez-Decampeneere D, et al. (1983) Pharmacokinetics and distribution of a biodegradable drug-carrier. International Journal of Pharmaceutics 15: 335-345.

12. Yuan SY, Rigor RR (2010) The endothelial barrier. Regulation of Endothelial Barrier Function. San Rafael, CA: Morgan & Claypool Life Sciences.

13. Li W, Nicol F, Szoka FC, Jr. (2004) GALA: a designed synthetic pH-responsive amphipathic peptide with applications in drug and gene delivery. Adv Drug Deliv Rev 56: 967-985.

14. Sasaki K, Kogure K, Chaki S, Nakamura Y, Moriguchi R, et al. (2008) An artificial virus-like nano carrier system: enhanced endosomal escape of nanoparticles via synergistic action of pH-sensitive fusogenic peptide derivatives. Anal Bioanal Chem 391: 2717-2727.

15. Choi SH, Choi K, Chan Kwon I, Ahn HJ (2010) The incorporation of GALA peptide into a protein cage for an acid-inducible molecular switch. Biomaterials 31: 5191-5198.

16. Nakase I, Kogure K, Harashima H, Futaki S (2011) Application of a fusiogenic peptide GALA for intracellular delivery. Methods Mol Biol 683: 525-533.

17. Nakase I, Futaki S (2015) Combined treatment with a pH-sensitive fusogenic peptide and cationic lipids achieves enhanced cytosolic delivery of exosomes. 5: 10112.

18. Sato Y, Nakamura T, Yamada Y, Harashima H (2016) Development of a multifunctional envelope-type nano device and its application to nanomedicine. Journal of Controlled Release 244, Part B: 194-204.
19. Kusumoto K, Akita H, Ishitsuka T, Matsumoto Y, Nomoto T, et al. (2013) Lipid envelope-type nanoparticle incorporating a multifunctional peptide for systemic siRNA delivery to the pulmonary endothelium. ACS Nano 7: 7534-7541.
20. Kusumoto K, Akita H, Santiwarangkool S, Harashima H (2014) Advantages of ethanol dilution method for preparing GALA-modified liposomal siRNA carriers on the in vivo gene knockdown efficiency in pulmonary endothelium. Int J Pharm 473: 144-147.
21. Akita H, Ishiba R, Hatakeyama H, Tanaka H, Sato Y, et al. (2013) A neutral envelope-type nanoparticle containing pH-responsive and SS-cleavable lipid-like material as a carrier for plasmid DNA. Adv Healthc Mater 2: 1120-1125.
22. Sakurai Y, Matsuda T, Hada T, Harashima H (2015) Efficient Packaging of Plasmid DNA Using a pH Sensitive Cationic Lipid for Delivery to Hepatocytes. Biological and Pharmaceutical Bulletin 38: 1185-1191.
23. Yamada Y, Tabata M, Yasuzaki Y, Nomura M, Shibata A, et al. (2014) A nanocarrier system for the delivery of nucleic acids targeted to a pancreatic beta cell line. Biomaterials 35: 6430-6438.
24. Hatakeyama H, Akita H, Ito E, Hayashi Y, Oishi M, et al. (2011) Systemic delivery of siRNA to tumors using a lipid nanoparticle containing a tumor-specific cleavable PEG-lipid. Biomaterials 32: 4306-4316.
25. Sato Y, Hatakeyama H, Sakurai Y, Hyodo M, Akita H, et al. (2012) A pH-sensitive cationic lipid facilitates the delivery of liposomal siRNA and gene silencing activity in vitro and in vivo. Journal of Controlled Release 163: 267-276.
26. Ren T, Song YK, Zhang G, Liu D (2000) Structural basis of DOTMA for its high intravenous transfection activity in mouse. Gene Therapy 7: 764-768.
27. Matsumoto M, Kishikawa R, Kurosaki T, Nakagawa H, Ichikawa N, et al. (2008) Hybrid vector including polyethylenimine and cationic lipid, DOTMA, for gene delivery. International Journal of Pharmaceutics 363: 58-65.
28. Zhang JS, Liu F, Huang L (2005) Implications of pharmacokinetic behavior of lipoplex for its inflammatory toxicity. Adv Drug Deliv Rev 57: 689-698.
29. Lonez C, Vandenbranden M, Elouahabi A, Ruysschaert JM (2008) Cationic lipid/DNA complexes induce TNF-alpha secretion in splenic macrophages. European Journal of Pharmaceutics and Biopharmaceutics 69: 817-823.
30. Ito Y, Kawakami S, Charoensit P, Higuchi Y, Hashida M (2009) Evaluation of proinflammatory cytokine production and liver injury induced by plasmid DNA/cationic liposome complexes with various mixing ratios in mice. European Journal of Pharmaceutics and Biopharmaceutics 71: 303-309.

31. Hatakeyama H, Murata M, Sato Y, Takahashi M, Minakawa N, et al. (2014) The systemic administration of an anti-miRNA oligonucleotide encapsulated pH-sensitive liposome results in reduced level of hepatic microRNA-122 in mice. Journal of Controlled Release 173: 43-50.
32. Sakurai Y, Hatakeyama H, Sato Y, Hyodo M, Akita H, et al. (2014) RNAi-mediated gene knockdown and anti-angiogenic therapy of RCCs using a cyclic RGD-modified liposomal-siRNA system. Journal of Controlled Release 173: 110-118.
33. Yamamoto S, Kato A, Sakurai Y, Hada T, Harashima H (2017) Modality of tumor endothelial VEGFR2 silencing-mediated improvement in intratumoral distribution of lipid nanoparticles. Journal of Controlled Release 251: 1-10.
34. Nakamura T, Miyabe H, Hyodo M, Sato Y, Hayakawa Y, et al. (2015) Liposomes loaded with a STING pathway ligand, cyclic di-GMP, enhance cancer immunotherapy against metastatic melanoma. Journal of Controlled Release 216: 149-157.
35. Immordino ML, Dosio F, Cattel L (2006) Stealth liposomes: review of the basic science, rationale, and clinical applications, existing and potential. Int J Nanomedicine 1: 297-315.
36. Dos Santos N, Allen C, Doppen AM, Anantha M, Cox KA, et al. (2007) Influence of poly(ethylene glycol) grafting density and polymer length on liposomes: relating plasma circulation lifetimes to protein binding. Biochim Biophys Acta 1768: 1367-1377.
37. Zamboni WC, Strychor S, Joseph E, Walsh DR, Zamboni BA, et al. (2007) Plasma, tumor, and tissue disposition of STEALTH liposomal CKD-602 (S-CKD602) and nonliposomal CKD-602 in mice bearing A375 human melanoma xenografts. Clin Cancer Res 13: 7217-7223.
38. Yang C, Gao S, Dagnæs-Hansen F, Jakobsen M, Kjems J (2017) Impact of PEG Chain Length on the Physical Properties and Bioactivity of PEGylated Chitosan/siRNA Nanoparticles in Vitro and in Vivo. ACS Applied Materials & Interfaces 9: 12203-12216.
39. Shah NB, Vercellotti GM, White JG, Fegan A, Wagner CR, et al. (2012) Blood–Nanoparticle Interactions and in Vivo Biodistribution: Impact of Surface PEG and Ligand Properties. Molecular Pharmaceutics 9: 2146-2155.
40. Pozzi D, Colapicchioni V, Caracciolo G, Piovesana S, Capriotti AL, et al. (2014) Effect of polyethyleneglycol (PEG) chain length on the bio-nano-interactions between PEGylated lipid nanoparticles and biological fluids: from nanostructure to uptake in cancer cells. Nanoscale 6: 2782-2792.
41. Hatakeyama H, Akita H, Harashima H (2013) The Polyethyleneglycol Dilemma: Advantage and Disadvantage of PEGylation of Liposomes for Systemic Genes and Nucleic Acids Delivery to Tumors. Biological and Pharmaceutical Bulletin 36: 892-899.
42. Ishitsuka T, Akita H, Harashima H (2011) Functional improvement of an IRQ-PEG-MEND for delivering genes to the lung. J Control Release 154: 77-83.
43. 楠本憲司 (2015) GALA 修飾ナノ粒子の肺血管内皮標的化メカニズム解明と核酸創剤への応用展開. 生命科学院: 北海道大学. 89 p.

44. Hyodo M, Sakurai Y, Akita H, Harashima H (2014) “Programmed packaging” for gene delivery. Journal of Controlled Release 193: 316-323.
45. Zhi D, Zhang S, Wang B, Zhao Y, Yang B, et al. (2010) Transfection Efficiency of Cationic Lipids with Different Hydrophobic Domains in Gene Delivery. Bioconjugate Chemistry 21: 563-577.
46. Shim MS, Kwon YJ (2008) Controlled Delivery of Plasmid DNA and siRNA to Intracellular Targets Using Ketalized Polyethylenimine. Biomacromolecules 9: 444-455.
47. Guo S, Huang L (2011) Nanoparticles Escaping RES and Endosome: Challenges for siRNA Delivery for Cancer Therapy. Journal of Nanomaterials 2011: 12.
48. Christie W (2017) Ether Lipids. AOCS Lipid Library. Urbana, IL, USA: The American Oil Chemists’ Society.
49. Heyes J, Palmer L, Bremner K, MacLachlan I (2005) Cationic lipid saturation influences intracellular delivery of encapsulated nucleic acids. Journal of Controlled Release 107: 276-287.
50. Bailey AL, Cullis PR (1997) Membrane Fusion with Cationic Liposomes: Effects of Target Membrane Lipid Composition. Biochemistry 36: 1628-1634.
51. Felgner JH, Kumar R, Sridhar CN, Wheeler CJ, Tsai YJ, et al. (1994) Enhanced gene delivery and mechanism studies with a novel series of cationic lipid formulations. Journal of Biological Chemistry 269: 2550-2561.
52. Akinc A, Querbes W, De S, Qin J, Frank-Kamenetsky M, et al. (2010) Targeted delivery of RNAi therapeutics with endogenous and exogenous ligand-based mechanisms. Mol Ther 18: 1357-1364.
53. Yan X, Kuipers F, Havekes LM, Havinga R, Dontje B, et al. (2005) The role of apolipoprotein E in the elimination of liposomes from blood by hepatocytes in the mouse. Biochem Biophys Res Commun 328: 57-62.
54. Hatters DM, Peters-Libeu CA, Weisgraber KH (2006) Apolipoprotein E structure: insights into function. Trends in Biochemical Sciences 31: 445-454.
55. Øie CI, Appa RS, Hilden I, Petersen HH, Gruhler A, et al. (2011) Rat liver sinusoidal endothelial cells (LSECs) express functional low density lipoprotein receptor-related protein-1 (LRP-1). Journal of Hepatology 55: 1346-1352.
56. Woodle MC, Matthay KK, Newman MS, Hidayat JE, Collins LR, et al. (1992) Versatility in lipid compositions showing prolonged circulation with sterically stabilized liposomes. Biochimica et Biophysica Acta (BBA) - Biomembranes 1105: 193-200.
57. Yan X, Scherphof GL, Kamps JAAM (2005) Liposome opsonization. Journal of Liposome Research 15: 109-139.
58. Fernandez-Megia E, Novoa-Carballal R, Quiñoá E, Riguera R (2007) Conjugation of Bioactive Ligands to PEG-Grafted Chitosan at the Distal End of PEG. Biomacromolecules 8: 833-842.

59. Guo J, Gao X, Su L, Xia H, Gu G, et al. (2011) Aptamer-functionalized PEG–PLGA nanoparticles for enhanced anti-glioma drug delivery. Biomaterials 32: 8010-8020.
60. Knudsen NØ, Schiffelers RM, Jorgensen L, Hansen J, Frokjaer S, et al. (2012) Design of cyclic RKKH peptide-conjugated PEG liposomes targeting the integrin α2β1 receptor. International Journal of Pharmaceutics 428: 171-177.
61. Shiokawa T, Hattori Y, Kawano K, Ohguchi Y, Kawakami H, et al. (2005) Effect of polyethylene glycol linker chain length of folate-linked microemulsions loading aclacinomycin A on targeting ability and antitumor effect in vitro and in vivo. Clin Cancer Res 11: 2018-2025.
62. Yamada A, Taniguchi Y, Kawano K, Honda T, Hattori Y, et al. (2008) Design of folate-linked liposomal doxorubicin to its antitumor effect in mice. Clinical Cancer Research 14: 8161-8168.
63. Maruyama K, Takizawa T, Yuda T, Kennel SJ, Huang L, et al. (1995) Targetability of novel immunoliposomes modified with amphipathic poly(ethylene glycol)s conjugated at their distal terminals to monoclonal antibodies. Biochim Biophys Acta 1234: 74-80.
64. Litzinger DC, Brown JM, Wala I, Kaufman SA, Van GY, et al. (1996) Fate of cationic liposomes and their complex with oligonucleotide in vivo. Biochim Biosys Act 1281: 139-149.
65. Mattfeld T, Mall G, Gharehbaghi H, Moller P (1990) Estimation of surface area and length with the orientator. Journal of Microscopy 159.
66. Kakudo T, Chaki S, Futaki S, Nakase I, Akaji K, et al. (2004) Transferrin-modified liposomes equipped with a pH-sensitive fusogenic peptide: an artificial viral-like delivery system. Biochemistry 43: 5618-5628.
67. Frisch B, Carrière M, Largeau C, Mathey F, Masson C, et al. (2004) A new triantennary galactose-targeted PEGylated gene carrier, characterization of its complex with DNA, and transfection of hepatoma cells. Bioconjug Chem 15: 754-764.
68. Blessing T, Kursa M, Holzhauser R, Kircheis R, Wagner E (2001) Different strategies for formation of pegylated EGF-conjugated PEI/DNA complexes for targeted gene delivery. Bioconjug Chem 12: 529-537.
69. Paranjpe PV, Chen Y, Kholodovych V, Welsh W, Stein S, et al. (2004) Tumor-targeted bioconjugate based delivery of camptothecin: design, synthesis and in vitro evaluation. J Control Release 100: 275-292.
70. Mammen M, Choi SK, Whitesides GM (1998) Polyvalent interactions in biological systems: Implications for design and use of multivalent ligands and inhibitors. Angew Chem Int Ed 37: 2754-2794.
71. Weis W, Brown JH, Cusack S, Paulson JC, Skehel JJ, et al. (1988) Structure of the influenza virus haemagglutinin complexed with its receptor, sialic acid. Nature 333: 426-431.
72. Edinger TO, Pohl MO, Stertz S (2014) Entry of influenza A virus: host factors and antiviral targets. Journal of General Virology 95: 263-277.

73. Kobayashi S, Nakase I, Kawabata N, Yu H-H, Pujals S, et al. (2009) Cytosolic Targeting of Macromolecules Using a pH-Dependent Fusogenic Peptide in Combination with Cationic Liposomes. Bioconjugate Chemistry 20: 953-959.
74. Chen J, Chen Z, Narasaraju T, Jin N, Liu L (2004) Isolation of highly pure alveolar epithelial type I and type II cells from rat lungs. Lab Invest 84: 727-735.
75. Gonzalez RF, Dobbs LG (2013) Isolation and Culture of Alveolar Epithelial Type I and Type II Cells from Rat Lungs. Methods in molecular biology (Clifton, NJ) 945: 145-159.
76. Yamamoto K, Ferrari JD, Cao Y, Ramirez MI, Jones MR, et al. (2012) Type I Alveolar Epithelial Cells Mount Innate Immune Responses during Pneumococcal Pneumonia. Journal of immunology (Baltimore, Md : 1950) 189: 2450-2459.
77. Wang LH, Rothberg KG, Anderson RG (1993) Mis-assembly of clathrin lattices on endosomes reveals a regulatory switch for coated pit formation. The Journal of Cell Biology 123: 1107.
78. Schnitzer JE, Oh P, Pinney E, Allard J (1994) Filipin-sensitive caveolae-mediated transport in endothelium: reduced transcytosis, scavenger endocytosis, and capillary permeability of select macromolecules. The Journal of Cell Biology 127: 1217.
79. Kerr MC, Teasdale RD (2009) Defining Macropinocytosis. Traffic 10: 364-371.
80. Koivusalo M, Welch C, Hayashi H, Scott CC, Kim M, et al. (2010) Amiloride inhibits macropinocytosis by lowering submembranous pH and preventing Rac1 and Cdc42 signaling. The Journal of Cell Biology.
81. Miller K, Shipman M, Trowbridge IS, Hopkins CR (1991) Transferrin receptors promote the formation of clathrin lattices. Cell 65: 621-632.
82. Orlandi PA, Fishman PH (1998) Filipin-dependent Inhibition of Cholera Toxin: Evidence for Toxin Internalization and Activation through Caveolae-like Domains. The Journal of Cell Biology 141: 905.
83. van Dam EM, Stoorvogel W (2002) Dynamin-dependent Transferrin Receptor Recycling by Endosome-derived Clathrin-coated Vesicles. Molecular Biology of the Cell 13: 169-182.
84. Commisso C, Davidson SM, Soydaner-Azeloglu RG, Parker SJ, Kamphorst JJ, et al. (2013) Macropinocytosis of protein is an amino acid supply route in Ras-transformed cells. Nature 497: 633-637.
85. Kolate A, Baradia D, Patil S, Vhora I, Kore G, et al. (2014) PEG - A versatile conjugating ligand for drugs and drug delivery systems. J Control Release 192C: 67-81.
86. Pusztaszeri MP, Seelentag W, Bosman FT (2006) Immunohistochemical Expression of Endothelial Markers CD31, CD34, von Willebrand Factor, and Fli-1 in Normal Human Tissues. Journal of Histochemistry and Cytochemistry 54: 385-395.
87. Turley SJ, Cremasco V, Astarita JL (2015) Immunological hallmarks of stromal cells in the tumour microenvironment. Nat Rev Immunol 15: 669-682.

88. Marelli-Berg FM, Clement M, Mauro C, Caligiuri G (2013) An immunologist's guide to CD31 function in T-cells. Journal of Cell Science 126: 2343-2352.
89. Zaynagetdinov R, Sherrill TP, Kendall PL, Segal BH, Weller KP, et al. (2013) Identification of Myeloid Cell Subsets in Murine Lungs Using Flow Cytometry. American Journal of Respiratory Cell and Molecular Biology 49: 180-189.
90. Chuquimia OD, Petursdottir DH, Rahman MJ, Hartl K, Singh M, et al. (2012) The Role of Alveolar Epithelial Cells in Initiating and Shaping Pulmonary Immune Responses: Communication between Innate and Adaptive Immune Systems. PLOS ONE 7: e32125.
91. McElroy MC, Kasper M (2004) The use of alveolar epithelial type I cell-selective markers to investigate lung injury and repair. European Respiratory Journal 24: 664-673.
92. Barth K, Blasche R, Kasper M (2010) T1alpha/podoplanin shows raft-associated distribution in mouse lung alveolar epithelial E10 cells. Cellular Physiology and Biochemistry 25: 103-112.
93. Maina JN, West JB (2005) Thin and strong! The bioengineering dilemma in the structural and functional design of the blood-gas barrier. Physiological Reviews 85: 811-844.
94. Crapo JD, Barry BE, Gehr P, Bachofen M, Weibel ER (1982) Cell number and cell characteristics of the normal human lung. American Review of Respiratory Disease 126: 332-337.
95. Sohrab S, Petrusca DN, Lockett AD, Schweitzer KS, Rush NI, et al. (2009) Mechanism of α-1 antitrypsin endocytosis by lung endothelium. The FASEB Journal 23: 3149-3158.
96. Rust MJ, Lakadamyali M, Zhang F, Zhuang X (2004) Assembly of endocytic machinery around individual influenza viruses during viral entry. Nat Struct Mol Biol 11: 567-573.
97. Chen C, Zhuang X (2008) Epsin 1 is a cargo-specific adaptor for the clathrin-mediated endocytosis of the influenza virus. Proceedings of the National Academy of Sciences 105: 11790-11795.
98. Sieczkarski SB, Whittaker GR (2002) Influenza Virus Can Enter and Infect Cells in the Absence of Clathrin-Mediated Endocytosis. Journal of Virology 76: 10455-10464.
99. de Vries E, Tscherne DM, Wienholts MJ, Cobos-Jiménez V, Scholte F, et al. (2011) Dissection of the Influenza A Virus Endocytic Routes Reveals Macropinocytosis as an Alternative Entry Pathway. PLOS Pathogens 7: e1001329.
100. Falkowska-Hansen B, Falkowski M, Metharom P, Krunic D, Goerdt S (2007) Clathrin-coated vesicles form a unique net-like structure in liver sinusoidal endothelial cells by assembling along undisrupted microtubules. Experimental Cell Research 313: 1745-1757.
101. Tiruppathi C, Song W, Bergenfeldt M, Sass P, Malik AB (1997) Gp60 Activation Mediates Albumin Transcytosis in Endothelial Cells by Tyrosine Kinase-dependent Pathway. Journal of Biological Chemistry 272: 25968-25975.

102. Tiruppathi C, Naqvi T, Wu Y, Vogel SM, Minshall RD, et al. (2004) Albumin mediates the transcytosis of myeloperoxidase by means of caveolae in endothelial cells. Proceedings of the National Academy of Sciences of the United States of America 101: 7699-7704.
103. Chanthick C, Kanlaya R, Kiatbumrung R, Pattanakitsakul S-n, Thongboonkerd V (2016) Caveolae-mediated albumin transcytosis is enhanced in dengue-infected human endothelial cells: A model of vascular leakage in dengue hemorrhagic fever. Scientific Reports 6: 31855.
104. Di Pasquale G, Chiorini JA (2006) AAV transcytosis through barrier epithelia and endothelium. Molecular Therapy 13: 506-516.
105. Lockett AD, Brown MB, Santos-Falcon N, Rush NI, Oueini H, et al. (2014) Active Trafficking of Alpha 1 Antitrypsin across the Lung Endothelium. PLOS ONE 9: e93979.
106. Ye D, Raghnaill MN, Bramini M, Mahon E, Aberg C, et al. (2013) Nanoparticle accumulation and transcytosis in brain endothelial cell layers. Nanoscale 5: 11153-11165.
107. Armstrong SM, Khajoee V, Wang C, Wang T, Tigdi J, et al. (2012) Co-Regulation of Transcellular and Paracellular Leak Across Microvascular Endothelium by Dynamin and Rac. The American Journal of Pathology 180: 1308-1323.
108. Ham AS, Klibanov AL, Lawrence MB (2009) Action at a distance: lengthening adhesion bonds with poly(ethylene glycol) spacers enhances mechanically stressed affinity for improved vascular targeting of microparticles. Langmuir 25: 10038-10044.
109. Sawant RR, Sawant RM, Kale AA, Torchilin VP (2008) The architecture of ligand attachment to nanocarriers controls their specific interaction with target cells. Journal of Drug Targeting 16: 596-600.
110. and JBW, Mathieu-Costello O (1999) STRUCTURE, STRENGTH, FAILURE, AND REMODELING OF THE PULMONARY BLOOD-GAS BARRIER. Annual Review of Physiology 61: 543-572.
111. Mühlfeld C, Rothen-Rutishauser B, Vanhecke D, Blank F, Gehr P, et al. (2007) Visualization and quantitative analysis of nanoparticles in the respiratory tract by transmission electron microscopy. Particle and Fibre Toxicology 4: 11.
112. McIntosh DP, Tan X-Y, Oh P, Schnitzer JE (2002) Targeting endothelium and its dynamic caveolae for tissue-specific transcytosis in vivo: A pathway to overcome cell barriers to drug and gene delivery. Proceedings of the National Academy of Sciences of the United States of America 99: 1996-2001.
113. Mehta D, Malik AB (2005) Signaling Mechanisms Regulating Endothelial Permeability. Physiological Reviews 86: 279.
114. Li C-H, Shyu M-K, Jhan C, Cheng Y-W, Tsai C-H, et al. (2015) Gold Nanoparticles Increase Endothelial Paracellular Permeability by Altering Components of Endothelial Tight Junctions, and Increase Blood-Brain Barrier Permeability in Mice. Toxicological Sciences 148: 192-203.

115. El-Sayed A, Harashima H Endocytosis of Gene Delivery Vectors: From Clathrin-dependent to Lipid Raft-mediated Endocytosis. Molecular Therapy 21: 1118-1130.
116. Parton RG, del Pozo MA (2013) Caveolae as plasma membrane sensors, protectors and organizers. Nat Rev Mol Cell Biol 14: 98-112.
117. Oh P, Borgstrom P, Witkiewicz H, Li Y, Borgstrom BJ, et al. (2007) Live dynamic imaging of caveolae pumping targeted antibody rapidly and specifically across endothelium in the lung. Nat Biotech 25: 327-337.
118. Azizi PM, Zyla RE, Guan S, Wang C, Liu J, et al. (2015) Clathrin-dependent entry and vesicle-mediated exocytosis define insulin transcytosis across microvascular endothelial cells. Molecular Biology of the Cell 26: 740-750.
119. Abulrob A, Sprong H, En Henegouwen PVB, Stanimirovic D (2005) The blood–brain barrier transmigrating single domain antibody: mechanisms of transport and antigenic epitopes in human brain endothelial cells. Journal of Neurochemistry 95: 1201-1214.

# Acknowledgements

This page is where you would acknowledge all those who helped you with your academic research. This is not necessarily where you would recognize loved ones who supported you during your studies. That would be more appropriately done in an optional Dedication page. First of all, I would like to thank Prof. Hideyoshi Harashima for giving me a great opportunity to conduct the gene delivery research in our laboratory. Secondly, I would like to appreciate Prof. Hidekata Akita from Chiba University. He has been the dedicating supervisor since I first came to the laboratory in 2012. I have learned how to develop scientific thinking and research design from Prof. Harashima, and Prof. Akita. Next, I would like to thank Assist. Prof. Yusuke Sato for supporting the research using YSK lipid series, and supervising me after Prof. Akita moved to Chiba University in 2016. I would also express gratitude toward Assoc. Prof. Yuma Yamada, Assist. Prof. Takashi Nakamura, Assist. Prof. Yu Sakurai and Assist. Prof. Ikramy Khalil for advice and feedback regarding the research during the seminar presentation. Furthermore, I would like to express my sincere thanks to lab colleagues and junior members for assistance and lab activities.

My Ph.D. project would not be successful if I did not give full supports from Department of Respiratory Medicine, Faculty of Medicine, Hokkaido University. I greatly appreciate Prof. Masaharu Nishimura, Assist. Prof. Masaru Suzuki and Dr. Hiroki Kimura for teaching animal techniques and clinical knowledge relating to respiratory diseases, as well as supporting facilities for animal experiments. I would also thank Miss Yoko Tani and Miss Yuka Sugiura for direct technical assistance in the experiments, as well as advice about private life in Hokkaido.

Not only academic professionals in Hokkaido University,but I would also like to express gratitude to Dr.Kenji Kusumoto from Taiho Pharmaceutical Co., Ltd. for providing previous experimental data and useful advice for my studies. Finally, I would express my thankfulness for my family for mental support and willpower since before coming to Japan.

Another series of my life has to end again. But, this end is the beginning for my new role in the society. I would apply the skills and experiences that I gained during the study in Hokkaido University, for building new knowledge and creating inventions which benefit the society.